Diamond & Related Materials 156 (2025) 112432

Contents lists available at ScienceDirect

Diamond & Related Materials

journal homepage: www.elsevier.com/locate/diamond

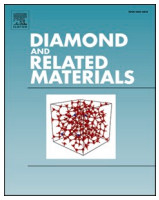

Non-covalent and covalent binding of proteins on ultrananocrystalline diamond films with different surface terminations☆

Rezvaneh Ghasemitabesh [a], Daniel Merker [a], Jan W. Bröckel [b], Daniela Bertinetti [b], Yahya Zakaria [c], Alexander Welle [d], Friedrich W. Herberg [b], Cyril Popov [a,*]

[a] Institute of Nanostructure Technologies and Analytics (INA), Center for Interdisciplinary Nanostructure Science and Technology (CINSaT), University of Kassel, Heinrich-Plett-Str. 40, 34132 Kassel, Germany
[b] Department of Biochemistry, Center for Interdisciplinary Nanostructure Science and Technology (CINSaT), University of Kassel, Heinrich-Plett-Str. 40, 34132 Kassel, Germany
[c] Thermo Fisher Scientific, The Felbridge Centre, Imberhorne Lane, East Grinstead, UK
[d] Karlsruhe Nano Micro Facility (KNMFi) and Institute of Functional Interfaces, Karlsruhe Institute of Technology, Hermann-von-Helmholtz-Platz 1, 76344 Eggenstein-Leopoldshafen, Germany

ARTICLE INFO

Keywords:
Ultrananocrystalline diamond
Protein immobilization
Biosensors
Surface termination
Nanostructuring
Fluorescence spectroscopy

ABSTRACT

The immobilization of proteins on solid surfaces is a critical aspect of biosensor development, offering enhanced sensitivity and specificity for molecular recognition. Ultrananocrystalline diamond (UNCD) films have emerged as a promising platform for protein immobilization due to their exceptional biocompatibility, chemical stability, and tunable surface properties. In this study, we investigate the non-covalent and covalent binding of green fluorescent protein (GFP) on nanostructured UNCD surfaces employing fluorescence spectroscopy to assess the efficiency of protein immobilization. The non-covalent binding was affected by the surface terminations (hydrogen, oxygen, and fluorine) rendered by different plasma modifications. The oxygen-terminated UNCD surfaces exhibited the highest efficiency attributed to favorable wettability and electrostatic interactions, revealed by zeta potential and contact angle measurements. The covalent immobilization via linker chemistry was studied for both GFP and anti-GFP nanobodies with the variation of the GFP concentration within the range of 10 μM – 10 pM. Milk powder was applied as a blocker to minimize the non-covalent binding of the target proteins. The intensity of the fluorescence signal decreased with the GFP concentration and below 1–10 nM approached that of the buffer control samples. The individual steps of the protein immobilization were investigated by zeta potential measurements, X-ray photoelectron spectroscopy (XPS) and time-of-flight secondary ion mass spectrometry (ToF-SIMS). Finally, a fluorescent dye-labeled nanobody was constructed as a reporter complex and applied to provide fluorescence signals distinguishable from those of GFP due to the different wavelengths. Such complexes combine the high specificity of the binding proteins with the bright and stable signal of the fluorescent dyes and can be implemented for realization of biosensors.

1. Introduction

Protein immobilization is a fundamental step in the development of all devices that take advantage of the wide variety of proteins and their unique properties. Biosensors, for example, rely on the immobilization of binding proteins with high specificity against a specific target to ensure that only the target creates a positive signal. These proteins can be enzymes or antibodies (immunoglobulins) and derivatives of the latter, such as nanobodies. Enzymes act upon substrate molecules and decrease the activation energy necessary for a chemical reaction to occur by stabilizing the transition state, i.e. they catalyze the reaction. The best-known enzyme biosensor is probably the glucose biosensor, which uses the reaction of glucose to glucono-δ-lactone in the presence of the enzyme glucose oxidase (GOD) [1]. In contrast to enzymes, which have evolved slowly, structural flexibility is a key feature of immunoglobulins [2]. After the infection of an organism with a pathogen, its adaptive immune system can produce highly specific antibodies. Antibodies mature in specificity over time, which is evidence of their high

☆ This article is part of a Special issue entitled: 'ICDCM2024' published in Diamond & Related Materials.

* Corresponding author.
E-mail address: popov@ina.uni-kassel.de (C. Popov).

https://doi.org/10.1016/j.diamond.2025.112432
Received 11 March 2025; Received in revised form 1 May 2025; Accepted 8 May 2025
Available online 9 May 2025

flexibility. Furthermore, not only the pathogen (e.g. bacterium, virus) itself but also a specific feature on its surface can be a target of the antibodies to bind to and mark it for the immune system [3,4]. For these reasons, antibodies have become the gold standard for biosensors when precise target recognition and capture are required, and a technique evolved from this is the immunoassay [5].

Immobilization of proteins on surfaces can generally be realized using two approaches. Covalent immobilization involves the creation of a chemical bond, while non-covalent immobilization is achieved by interactions between the protein and the surface such as electrostatic interactions, van der Waals forces or the hydrophobic effect. Both approaches have their advantages and disadvantages, and which method is used depends on various properties of the protein, the surface, the application and the conditions for the application. The glucose biosensor mentioned above, for example, is realized by non-covalently immobilized GOD enzymes [1]. A covalent immobilization would be more time-consuming and expensive and is not necessary for the intended application. On the other hand, the immobilization of enzymes in a bioreactor can be advantageous to avoid mixing the enzyme with the substrate/product solution and to reduce the effort required for purification afterwards [6]. Besides the economic and process related considerations, the effect of immobilization on the immobilized protein itself should be kept in mind. Both covalent and non-covalent immobilization can affect the efficiency of enzymes or binding proteins simply due to steric hindrance and blockade of the active or binding sites of the proteins by the site used for immobilization [7]. Binding proteins are highly directional, i.e. the interaction with the substrate/antigen is established at a certain area of the protein [8,9]. If covalent binding or non-covalent interactions for immobilization occur near that region, it can lead to inactivation [10]. Additionally, conformational change may be required to form a bond and could be obstructed [11,12]. However, there are also reports that immobilization caused a significant increase in enzyme activity and stability against environmental impacts [13–16].

The same interactions that immobilize a protein non-covalently also dictate its three-dimensional structure. A protein is functional only when its structure is correct, governed by the process of protein folding [13]. The three-dimensional structure of a protein is determined by the amino acid sequence (primary structure) and by the interactions between the amino acid backbone (secondary structure) as well as interactions of the side chains (polar with charged or uncharged side chains and hydrophobic side chains) and the surrounding environment, which leads to the formation of stabilized domains. Those domains interact with each other within the tertiary structure and finally it can happen that several amino acid chains (each one then denoted as a sub-unit) interact forming the quaternary structure. Tertiary and quaternary structure may be stabilized by covalent interactions between cysteine residues forming disulfide bonds. Besides this, each of these steps is driven by interactions that are also responsible for non-covalent immobilization (electrostatic, van der Waals forces and hydrophobic effect) [17,18]. Interaction with the surface can therefore result in denaturation of the protein, for example when the hydrophobic core of the protein – formed during its folding due to the interaction with the typically aqueous environment in cells or bacteria – is exposed to a highly hydrophobic surface [18]. For covalent immobilization, the surface must be prepared in such a way that it can form a chemical bond with the protein. For this purpose, the surface is usually functionalized to introduce terminal functional groups that serve as the basis for chemical coupling [19]. In the protein, suitable functional groups for immobilization attempts can be found on its N- or C-terminus (amino and carboxyl groups, respectively) and on the side chains of the amino acids (e.g. amino group for lysine, carboxyl group for glutamic acid, hydroxyl group for serine and thiol group for cysteine), if they are accessible to reactions. Coupling routes to immobilize proteins on surfaces are, for example, the EDC/NHS (carbodiimide and N-hydroxysuccinimide) route to establish a bond between a carboxyl group and an amino group [20], the glutaraldehyde coupling between two amino groups [21] or the ring-opening reaction between an epoxy group and a thiol or an amino group [22,23]. For all approaches it must be considered that introducing functional groups on the surface via plasma or chemical treatment is accompanied by changing the surface chemistry, charge state and wetting properties with the above-mentioned possible effects on the immobilization target. In summary, one must consider the protein to be immobilized as well as the properties of the surface and the aspired application. Educated presumptions can be made in advance but usually qualitative and quantitative experiments are required to evaluate the best combination of protein and surface.

Diamond is renowned for its exceptional biocompatibility, making it an attractive option for applications such as cell incubation and protein immobilization [24–26]. Its versatility is another key advantage, as its surface chemistry can be modified through plasma or photochemical treatment. Applying fluorine, ammonia or oxygen containing plasma, highly hydrophobic (in the first case) or hydrophilic surfaces (in the other two cases) can be generated in just minutes. The process also introduces functional groups on the surface, providing reactive sites for further chemical coupling [27]. Additionally, diamond's robust resistance to harsh reaction conditions and aggressive chemicals allows for further functionalization through various chemical reactions [27]. Diamond surfaces have previously been functionalized with covalently immobilized antibodies. For instance, the surface of a polycrystalline boron-doped diamond electrode was modified with an antibody targeting the influenza virus. This impedance biosensor demonstrated high sensitivity, detecting fewer than 10 virus particles, and significantly reduced analysis time compared to traditional methods, like polymerase chain reaction (PCR) and enzyme-linked immunosorbent assay (ELISA) [28]. In another study, boron-doped ultrananocrystalline diamond (UNCD) surface was functionalized with antibodies against *E. coli* to create an impedance biosensor for bacterial detection. UNCD was selected to minimize electrode fouling and the results showed improved selectivity, sensitivity, and signal reproducibility [29]. Immobilization of proteins onto modified diamond surfaces has been documented for a variety of proteins, including cytochrome C, albumin, myoglobin [30], lysozyme [31], and alcohol dehydrogenase [32]. In all cases, the proteins were not denatured, and the enzymes exhibited good or even enhanced activity when adsorbed onto the surface, compared to their free form. In a study conducted by our group, we compared the hydrolytic activity of a lipase on two different substrates – one small and one larger – immobilized either covalently or non-covalently on structured UNCD surfaces [33]. The lipase was non-covalently immobilized using different surface terminations: hydrophilic oxygen, hydrophobic hydrogen, or highly hydrophobic fluorine. Our results demonstrated that non-covalent immobilization on fluorine-terminated UNCD surfaces was the most efficient. Additionally, we found that the immobilized lipase exhibited a clear preference for the smaller substrate, suggesting that the proximity to the surface influenced its activity.

Employing dry etching techniques, diamond surfaces can be structured to increase surface area, thus improving immobilization efficiency. In a recent study, we showed through quantitative fluorescence imaging that a nanostructured UNCD surface can accommodate more proteins (specifically green fluorescent protein, GFP) than an unstructured UNCD surface [34]. This was observed for both covalent and non-covalent protein immobilization. The current study aims to expand these findings by investigating the direct immobilization of GFP and GFP-specific nanobodies, followed by the capture of GFP from solutions with different concentrations on structured and unstructured UNCD surfaces using both covalent and non-covalent immobilization strategies. The application of GFP is advantageous since the efficiency of its immobilization can be directly studied by the intensity of the fluorescence signal, on one side, but can also serve as an indicator for any structural changes during the coupling which will lead to cease of the fluorescence, on the other. Nanobodies (NBs) (also single-domain antibodies) were applied as GFP-binding proteins. These are engineered fragments of heavy chain antibodies from members of the camelid

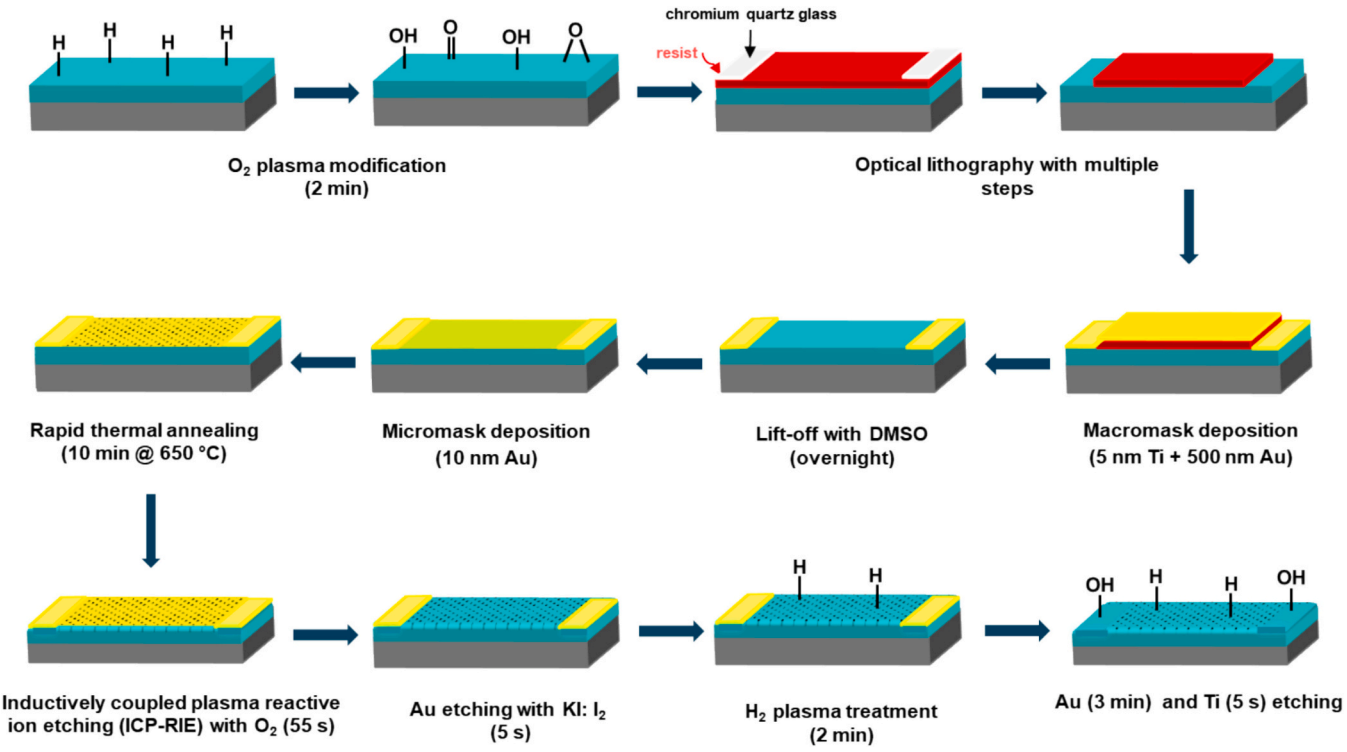

Fig. 1. Individual steps for the preparation of nanostructured H-terminated sensor fields surrounded by O-terminated flat UNCD surface.

family like Llamas or Alpacas or the shark family, yet they contain the complete antigen-binding region, and are about 10 times smaller in size (typically 10–15 kDa) than antibodies (150 kDa). They often show a higher stability against heat denaturation and denaturants compared to antibodies. At the same time their binding affinity and specificity are comparable. These unique biophysical properties, their small size and the possibility for production of novel nanobodies against affinity tags make them particularly attractive for applications as capturing agents and ligands in biosensing and diagnostic assays [35,36]. Finally, a fluorescent dye-labeled nanobody was developed as a reporter complex to provide fluorescence signals distinguishable from those of GFP due to the different excitation and emission wavelengths. Such complexes combine the high specificity of the binding proteins with the bright and stable signal of the fluorescent dyes. Furthermore, the use of fluorescently labeled nanobodies can facilitate multiplexing, enabling the simultaneous detection of multiple targets, which is essential for complex biological studies and comprehensive diagnostic assays [37,38]. This concept is intended for application in our next-generation biosensor, designed as a UNCD-based biosensor for time-resolved detection of neuropeptides, like pigment dispersing factor (PDF), released from clock cells of a model organism.

2. Experimental

2.1. Deposition, surface modifications and nanostructuring of UNCD films

The UNCD films used in this work were prepared by microwave plasma assisted chemical vapor deposition (MWCVD). 3-inch silicon (100) wafers were used as substrates, they were pretreated prior to the deposition to increase the nucleation density. Initially, they were submerged in buffered etch solution (NH_4F:HF = 7:1) for 35 s to remove the native SiO_2 layer. After rinsing with deionized water and drying in N_2 flow the substrates were ultrasonically treated in a diamond slurry *Opal Seeds* (Adámas Nanotechnologies) diluted in methanol (slurry:methanol = 1:3) for 30 min. Subsequently they were cleaned with acetone and isopropanol for 90 s each in the ultrasonic bath with N_2 drying in-between and after the end of the cleaning. The pretreated substrates were placed in the MWCVD setup (ASTeX) which was evacuated to a base pressure of around 4×10^{-3} mbar. Afterwards the substrates were heated to around 570 °C and subsequently the gas mixture of 17 vol% CH_4 and 83 vol% N_2 was introduced into the reaction chamber with a total flow of 300 sccm. The MW plasma power was set to 800 W and the working pressure was stabilized at around 30 mbar. After 6 h deposition UNCD layers with thickness of ca. 1–1.2 μm were achieved which corresponded to average growth rate of 3.5 nm min^{-1}. The coated substrates were cut into pieces with different sizes for further processing and characterization.

The as-grown UNCD films possess hydrogen-terminated surface which can be altered by the application of highly reactive species, e.g. in plasma conditions. In order to study the effect of the surface termination on the non-covalent binding of proteins, oxygen- and fluorine-terminated UNCD surfaces were prepared by plasma processes. Oxygen plasma treatment was performed in a plasma asher type 200-G (PVA TePla AG) at pressure of 0.7 mbar and microwave power of 150 W for 2 min. Modification with fluorine was achieved in an inductively coupled plasma reactive-ion etching (ICP-RIE) setup Plasmalab 100 (Oxford Instruments) applying trifluoromethane (CHF_3) with a flow of 25 sccm, pressure of 25 mTorr (33×10^{-3} mbar) and 50 W rf power for 30 s. The same setup was used to restore the hydrogen termination after nanostructuring (see below), which is required for the photochemical attachment of ω-alkenes as linker molecules [39,40]. In this case hydrogen gas flow of 20 sccm, pressure of 10 mTorr (13×10^{-3} mbar) and rf power of 200 W were applied for 2 min.

A detailed description of the UNCD nanostructuring process implemented also in the current work to increase the surface area for enhancement of protein immobilization can be found in our previous publication [34]; a scheme with the individual steps can be seen in Fig. 1. Briefly, after cleaning with acetone and isopropanol the 1.5×1.5 cm^2 samples were treated with oxygen plasma to achieve O-termination of the whole surface before the sensor fields (500×500 μm^2 squares) were defined in photoresist by photolithography. Afterwards, 5 nm

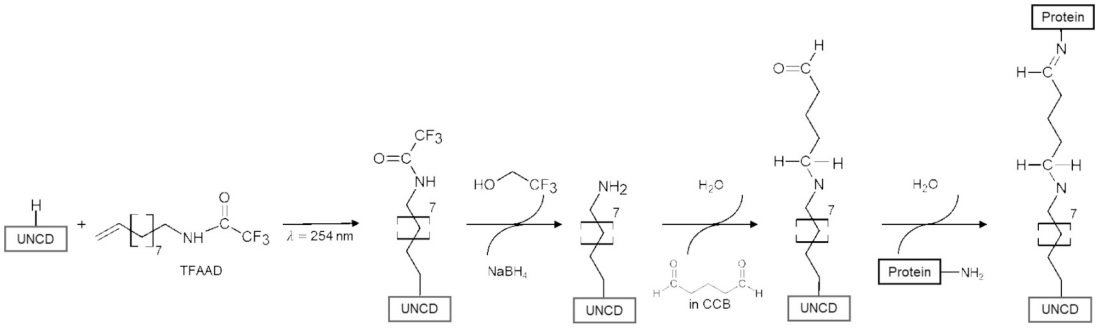

Fig. 2. Covalent immobilization of proteins (GFP and nanobodies) on UNCD surface.

titanium as adhesion promoter and 500 nm gold were electron-beam evaporated on top of the remained resist structure, the latter was lift-off with dimethyl sulfoxide (DMSO) overnight leaving the gold *macromask* on the UNCD surface. As next, 10 nm gold film was deposited and subjected to rapid thermal annealing, resulting in dewetting of the film and formation of gold islands. They served as a *micromask* for the following ICP-RIE with oxygen of the UNCD leading to its nanostructuring with wrinkles of ca. 100 nm height. The *micromask* was removed by wet chemical etching with KI/I_2 solution and the sample was exposed to hydrogen plasma in the ICP-RIE setup to restore the H-termination of the UNCD necessary for the functionalization with linker molecules. Finally, the *macromask* was removed with KI/I_2 solution and Ti-Etch. The finalized samples were cut into 9 pieces with a size of about 4×4 mm^2, each containing 9 sensor fields with a nanostructured H-terminated surface surrounded by areas of O-terminated unstructured UNCD. For some measurements where larger areas were required (zeta potential, contact angle, XPS, ToF-SIMS.), larger samples were cut, their entire surface was nanostructured and afterwards subjected to plasma modifications and protein immobilization.

2.2. Non-covalent binding of GFP on nanostructured UNCD surfaces with different terminations

Nanostructured 4×4 mm^2 UNCD samples were subjected to surface modifications with H_2, O_2 and CHF_3 plasmas under the conditions mentioned above in order to study the unspecific interactions of GFP with differently terminated surfaces. The H-, O- and F-terminated UNCD samples were glued with high vacuum grease to the bottom of a plastic cell culture dish with a diameter of 4 cm to avoid movement of the samples during incubation in GFP solutions (His-tagged GFPmut2 variant [41], $\lambda_{absorption,\ max} = 481$ nm and $\lambda_{emission,\ max} = 507$ nm, 10 μg mL^{-1} in phosphate-buffered saline (PBS) with pH 7.3, prepared and characterized as described in [42]) with various concentrations for 20 h being constantly shaken with approximately 80 rpm at 4 °C. Eight GFP concentrations were used: 10 μM, 1 μM, 100 nM, 30 nM, 10 nM, 3 nM, 1 nM, and 500 pM. After the incubation, the samples were washed twice with PBS-Tween 20 (Polysorbate 20, 0.05 %) and once with PBS for 2 min each under constant orbital shaking to remove GFP molecules weakly adsorbed on the surface. Then, fluorescence measurements were conducted using a microplate reader CLARIOstar (BMG Labtech) with a 320–840 nm variable filter monochromator for excitation and detection; for the GFP measurements in the current work $\lambda_{excitation} = 470 \pm 15$ nm and $\lambda_{detection} = 520 \pm 20$ nm were used. The samples were placed in black non-transparent 96-well microtiter plates with well diameter of 7 mm where their fixation was not necessary (HTRF black, Packard BioScience Ltd.). PBS was used both as buffer and as control sample during these measurements. The device was operated in fluorescence intensity (FI) mode with a matrix scan applied, which divided the well into a matrix of individual measuring points. Since 30×30 matrix was used, 900 measurement points per well were conducted with 4 mm scan diameter and pixel size ca. 133×133 μm^2 giving a spatial resolution of the fluorescence in the well and consequently on the sample. The average fluorescence over each well was determined and used to compare samples within a series of measurements. The multiplate reader applies auto-calibration based on the strongest fluorescence detected from the samples for each series which allows the direct comparison of their fluorescence signals. The comparison of signal intensities between different series, however, is not reliable due to the different calibration for each of them.

2.3. Covalent binding of GFP on functionalized UNCD surfaces

The covalent immobilization of GFP on nanostructured H-terminated UNCD surfaces was performed according to the protocol taken from [39] and presented in our recent publication [34]. A 2:1 mixture of 10-trifluoroacetamidodec-1-ene (TFAAD, abcr GmbH, 97 % purity) and 1-dodecene (Sigma Aldrich) was dropped between the sample surface and a quartz glass slide (Quantum Design GmbH, transmission $T_{\lambda=254\ nm} \geq 90$ %) with 2 μL cm^{-2} surface density. Then the sample was irradiated for 10 h with UV light (BHK Inc., with $\lambda = 254$ nm and intensity of 7.5 mW cm^{-2} at 2.54 cm distance from sample surface) which induced covalent attachment of TFAAD on the UNCD surface. Afterwards the sample was cleaned with chloroform and ethanol by soaking the sample for 15 min. The deprotection of the amino group was performed by submerging the sample in 65 mM sodium borohydride ($NaBH_4$, Sigma Aldrich) in methanol for 6 h at 60 °C. After rinsing with methanol and deionized water, the sample was submerged in 3 % glutaraldehyde in cyanoborohydride coupling buffer (CCB) (both Sigma-Aldrich) for 4 h at RT to achieve aldehyde termination by reductive amination. The sample was rinsed with deionized water and dried in an oven for 30 min at 70 °C and immediately implemented for immobilization of proteins (Fig. 2). As described above, the samples were affixed, incubated in GFP solutions, washed (twice with PBS-Tween 20 (Polysorbate 20, 0.05 %) and once with PBS for 2 min each under constant orbital shaking) to remove any non-covalent bonded proteins from the surfaces and subsequently the fluorescence was measured. In the current work, GFP solutions with concentrations lower than those in a previous study [34] were applied in order to test the detection limit of immobilized proteins: 30 nM, 10 nM, 3 nM, 1 nM, 300 pM, 100 pM, 30 pM, and 10 pM.

2.4. Covalent immobilization of nanobodies on UNCD surfaces as GFP-binding proteins and application of blocker proteins

The route for covalent immobilization of GFP was implemented also for other proteins, namely two recombinant anti-GFP nanobodies (Patent EP4077372A1) with reference numbers CA12760 (Nb207) and CA16047 (Nb47) (2.3 mg/mL, stored in PBS pH 7.3, DNA provided by Prof. Jan Steyaert, VIB-VUB Center for Structural Biology, Brussels, Belgium), referred as NB0 and NB7 in the following. The UNCD samples, nanostructured and functionalized with TFAAD linker, were incubated with 1 μg mL^{-1} of each nanobody for 20 h at 4 °C under constant shaking at 80 rpm. As next, the samples were washed and incubated with milk

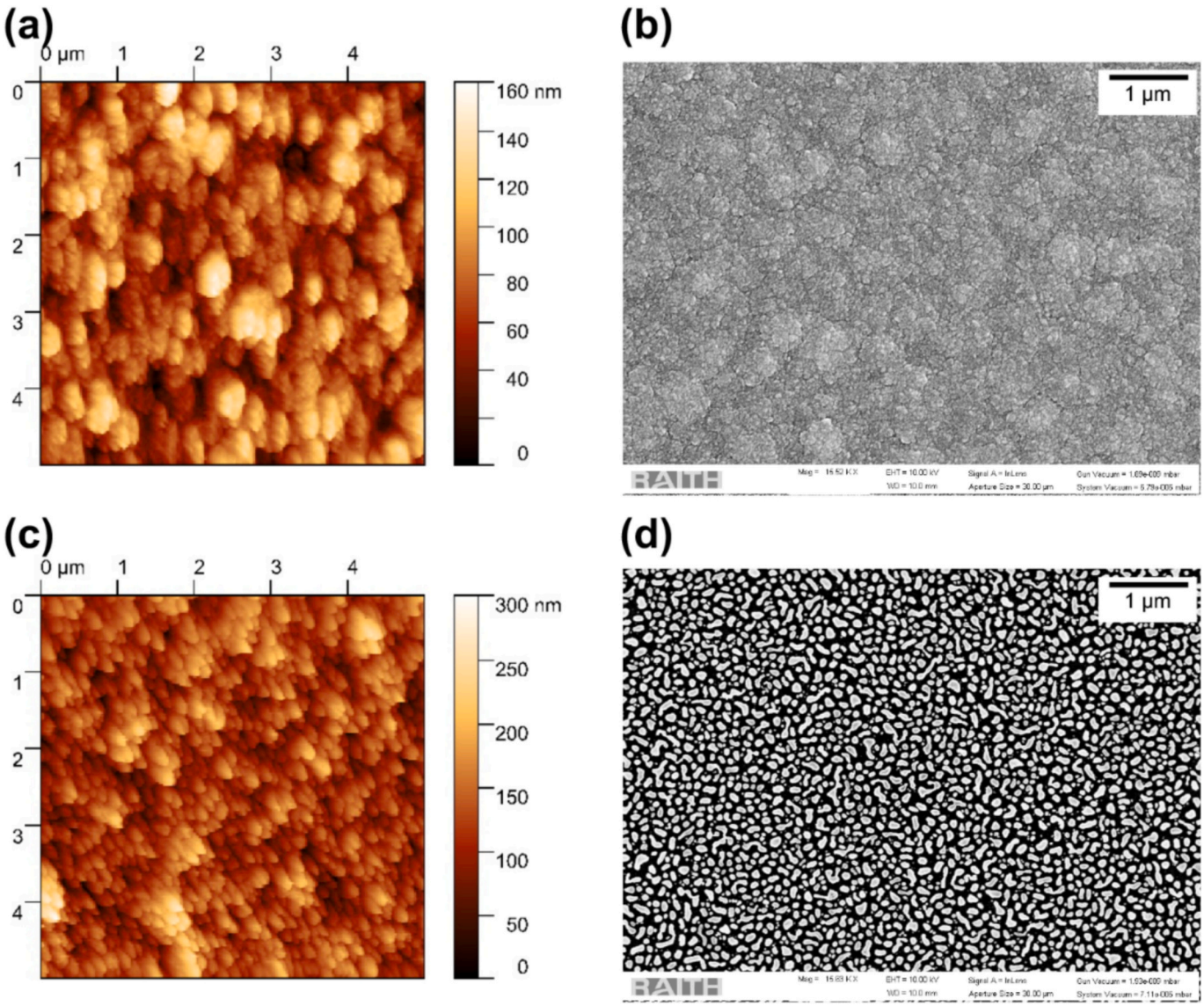

Fig. 3. (a) AFM image and (b) SEM micrograph of unstructured UNCD, (c) AFM image and (d) SEM micrograph of nanostructured UNCD surface.

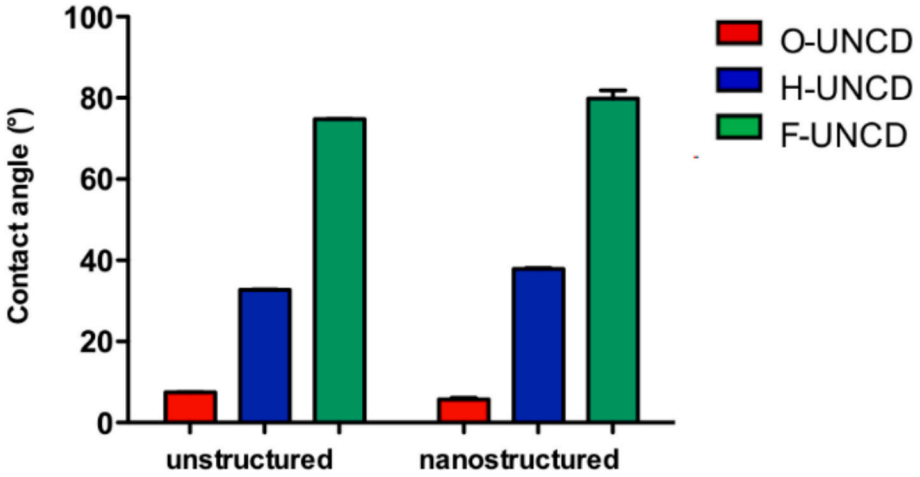

Fig. 4. Contact angles against water of unstructured and nanostructured UNCD surfaces with O-, H- and F-terminations ($N = 5$).

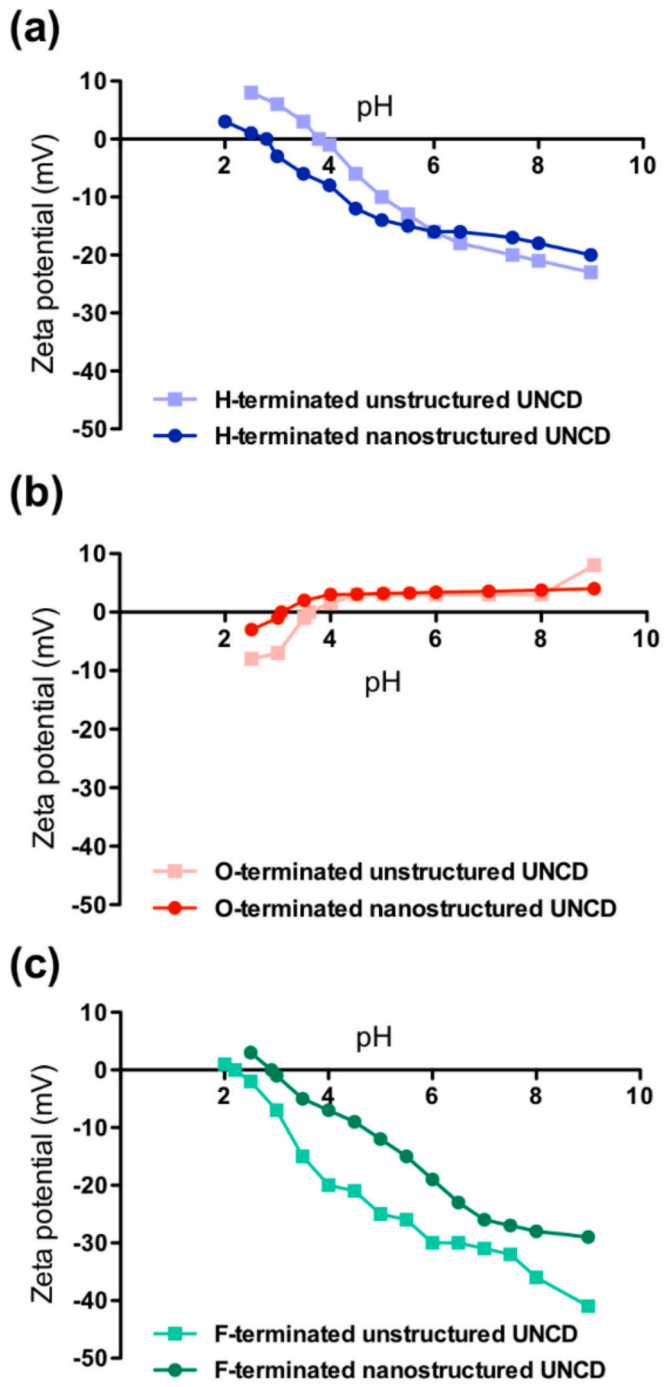

Fig. 5. Zeta potentials of unstructured and nanostructured UNCD surfaces with (a) O-, (b) H- and (c) F-terminations.

powder (2 wt% in PBS, milk powder in blotting grade, Carl Roth GmbH) for 30 min at 4 °C under constant shaking at 80 rpm. The milk powder was utilized as a blocker to occupy unspecific binding sites on the UNCD surface and minimize the non-covalent binding of GFP during the following interaction with the nanobodies. After another washing step, the samples were incubated for 10 min with GFP solutions with various concentrations: 5 μM, 1 μM, 100 nM, 30 nM, 10 nM, 3 nM, 1 nM, and 500 pM. Finally, the samples were washed with PBS to remove unbound proteins, ensuring that only GFP captured by the nanobodies remained on the surface before the fluorescence measurements carried out immediately after the incubation.

2.5. Preparation and application of fluorescent reporter complex

For the creation of a reporter complex GFP-binding nanobodies were labeled with fluorescent dye. Nanobody NB7 was conjugated with amine-reactive N-hydroxysuccinimidyl esters of Alexa Fluor fluorescent dye 647 (Thermo Fisher Scientific, Labeling Kit Cat. No. A20173) with principal excitation and emission maxima at 650 and 668 nm, respectively. The fluorescent labeled proteins were prepared, purified, and characterized according to instructions provided by the manufacturers (Thermo Fisher Scientific, Protein Labeling Kits User Guide (For Alexa Fluor, Pacific Blue, Fluorescein-EX, and Oregon Green 488); Pub. No. MAN0019835 A.0). 500 μL of NB7 was added to 50 μL of bicarbonate sodium to increase the pH values to provide suitable pH for reaction of the nanobodies with the dye. Then, the solution was transferred to a reactive dye vial and kept on stirrer overnight at 4 °C. The next day, the NB-dye solution was placed in a column for purification of labeled nanobodies from the non-labeled ones and free dye. The labeling efficiency and degree of labeling (DOL) were determined by UV–Vis spectrophotometry using absorbance measurements at 280 nm and 650 nm. In a series of experiments, GFP was captured from solutions with different concentrations (1 μM, 300 nM, 100 nM, 30 nM, 10 nM, 3 nM, 1 nM, 300 pM, 100 pM, and 30 pM) by 1 μg mL^{-1} nanobody (NB0) covalently immobilized on UNCD for 20 h at 4 °C under constant shaking at 80 rpm. Before capturing GFP by the nanobodies milk powder (2 wt% in PBS) was applied for 30 min at 4 °C under constant shaking at 80 rpm to prevent non-covalent binding of GFP on the UNCD surface. Subsequently, 1 μM nanobody (NB7) labeled with the fluorescent agent (reporter complex) was incubated for 10 min at 4 °C under constant shaking at 80 rpm to the captured GFP. Between each step, the samples were washed with PBS tween 20 and PBS 250 mM NaCl. The fluorescence measurements were carried out immediately after the incubation of the reporter complex on GFP- NB0 immobilized on UNCD surfaces. Since GFP and fluorescent agent have different excitation and emission wavelengths, their fluorescence intensity can be addressed independently.

2.6. Dynamic light scattering of applied proteins

The sizes of two nanobodies (NB0 and NB7), GFP and milk powder (as blocker) were measured using dynamic light scattering (DLS) technique with a Litesizer dynamic light scattering instrument (Anton Paar GmbH, Graz, Austria). The measurements were carried out at 25 °C, and the data were analyzed using Kalliope software to determine the size distribution of the proteins in terms of the hydrodynamic diameter. The reported size reflects the effective diameter of the protein particles in solution under the given conditions. In addition, the zeta potentials of these proteins were determined using an electrophoretic light scattering (ELS) setup. This technique applies an electric field to the protein sample in solution, and the resulting electrophoretic mobility is used to calculate the zeta potential, which provides insights into the surface charge and stability of the protein particles. Measurements were performed at 25 °C and the data were analyzed using the same software. The reported zeta potential values were expressed in millivolts (mV) and represent the average surface charge of the proteins under the experimental conditions. The concentration of nanobodies and GFP was 0.5 mg/mL, while the that of milk powder was 2 wt% for both measurements.

2.7. Zeta potential and contact angle measurements of differently prepared UNCD surfaces

The surface charge properties of the differently prepared UNCD samples were assessed by zeta potential measurements with SurPASS 3 (Anton Paar GmbH, Graz, Austria) in the pH range of 2.0–9.0. For each sample, two zeta potential/pH value functions were measured in 0.1 M KCl solution. The pH values were adjusted with 0.05 M NaOH solution to raise the pH to 9.0, or 0.05 M HCl to decrease it to 2.0. For statistical

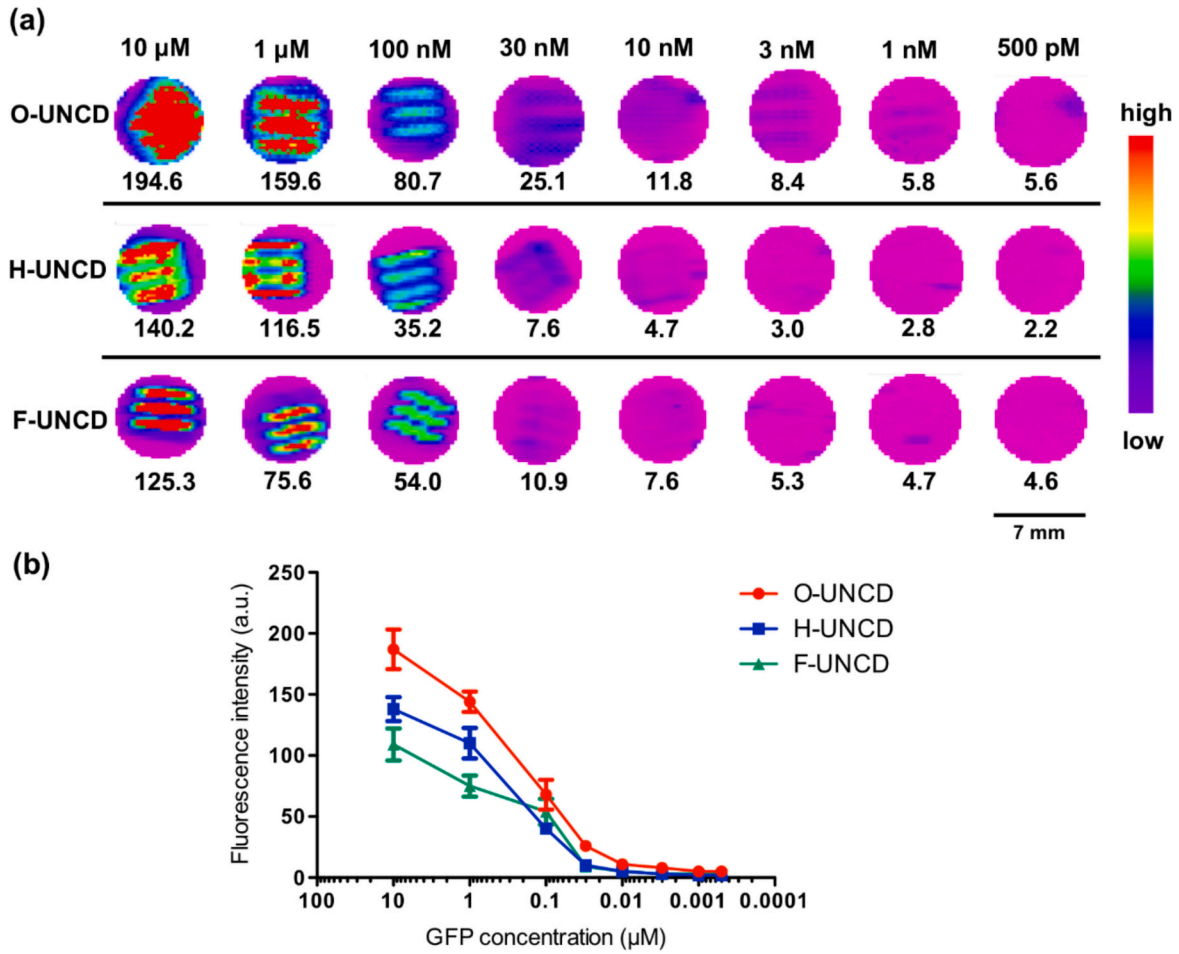

Fig. 6. Fluorescence measurements of nanostructured UNCD surfaces with O-, H- and F-terminations incubated with different GFP concentrations: (a) average fluorescence of the whole well in arbitrary units for one series of measurements (out of 5). The average fluorescence of PBS solution used as control (not shown here) was 2.1 a.u. (b) average fluorescence determined from all measured samples (N = 5).

Table 1
Measured zeta potentials and sizes of the proteins used in the current study together with literature data for the sizes of the proteins for comparison. *Most probably measured size of casein micelles, the reference given also concerns casein micelles.

	Zeta potential (mV)	Size (nm)	Size /reference (nm)
GFP	−9.5 ± 0.7	4.9 ± 1.3	4.0–4.2 [54,55]
NB0	−12.1 ± 0.5	2.9 ± 0.3	2.5–4.0 [56,57]
NB7	−7.3 ± 1.0	2.8 ± 0.5	
Milk powder*	−11.3 ± 0.9	194.0 ± 41.2	154–230 [58]

reasons, three streaming potentials were measured at each pH value. Single-sample method was implemented, i.e., only one sample was placed in the chamber, and an electric field was applied using a single electrode. Thus, the zeta potential was determined by measuring particle movement or changes in light intensity.

In a first group of experiments, the zeta potentials of unstructured and nanostructured UNCD surfaces with different terminations (O-, H-, and F-) were determined. The second group of samples for zeta potential measurements included: (1) nanostructured UNCD treated with H_2 plasma, (2) nanostructured UNCD treated with H_2 plasma, with photochemically attached TFAAD linker (after deprotection of $–NH_2$ group), (3) nanostructured UNCD treated with H_2 plasma, with photochemically attached TFAAD linker + glutaraldehyde, (4) nanostructured UNCD treated with H_2 plasma, with photochemically attached TFAAD linker + glutaraldehyde + GFP, (5) nanostructured UNCD treated with H_2 plasma, with photochemically attached TFAAD linker + glutaraldehyde + nanobody and (6) nanostructured UNCD treated with H_2 plasma, with photochemically attached TFAAD linker + glutaraldehyde + nanobody + blocker + GFP captured out of solution. All samples were prepared in size ca. 20 × 20 mm^2.

Contact angle measurements were performed to study the wettability of unstructured and nanostructured UNCD surfaces with different terminations. The contact angles against deionized water were monitored with an optical contact angle meter CAM 100 (KSV Instruments, Germany). A set of 15 images from the water droplet with 100 ms time gap between them were taken 1 s after the droplet was applied onto the surface and the average contact angle was calculated from them. The average contact angle with standard deviation was determined from five droplets applied on each sample.

2.8. XPS and ToF-SIMS measurements of differently prepared UNCD surfaces

X-ray photoelectron spectroscopy (XPS) measurements were conducted using K-Alpha+ by Thermo Fisher Scientific, with 50 eV as pass energy and 0.1 eV as step size. XPS instrument is calibrated using triple standards of Au/Ag/Cu and the measurements were referenced using C1s (C—C) at 284.8 eV.

Time-of-Flight Secondary Ion Mass Spectrometry (ToF-SIMS) was performed on a TOF.SIMS5 instrument (ION-TOF GmbH, Münster, Germany). The spectrometer is equipped with a Bi cluster primary ion

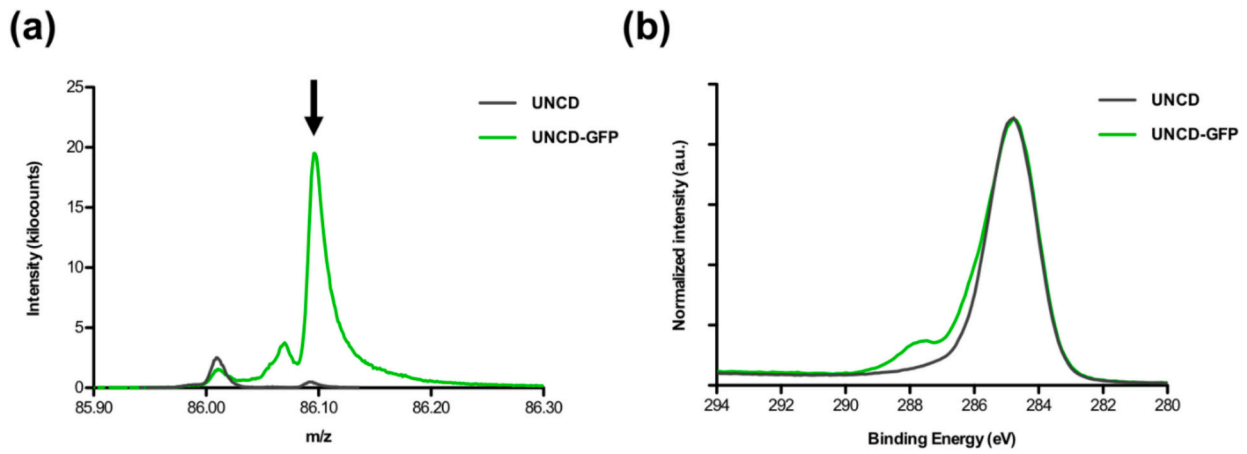

Fig. 7. (a) ToF-SIMS positive secondary ion $C_5H_{12}N^+$ from (iso-)leucine used as a marker for GFP non-covalently immobilized on H-terminated UNCD (green line), and pristine H-terminated nanostructured UNCD (black line); (b) Normalized XPS C 1 s spectra of the H-terminated nanostructured UNCD before (black line) and after (green line) non-covalent immobilization of GFP. (For interpretation of the references to colour in this figure legend, the reader is referred to the web version of this article.)

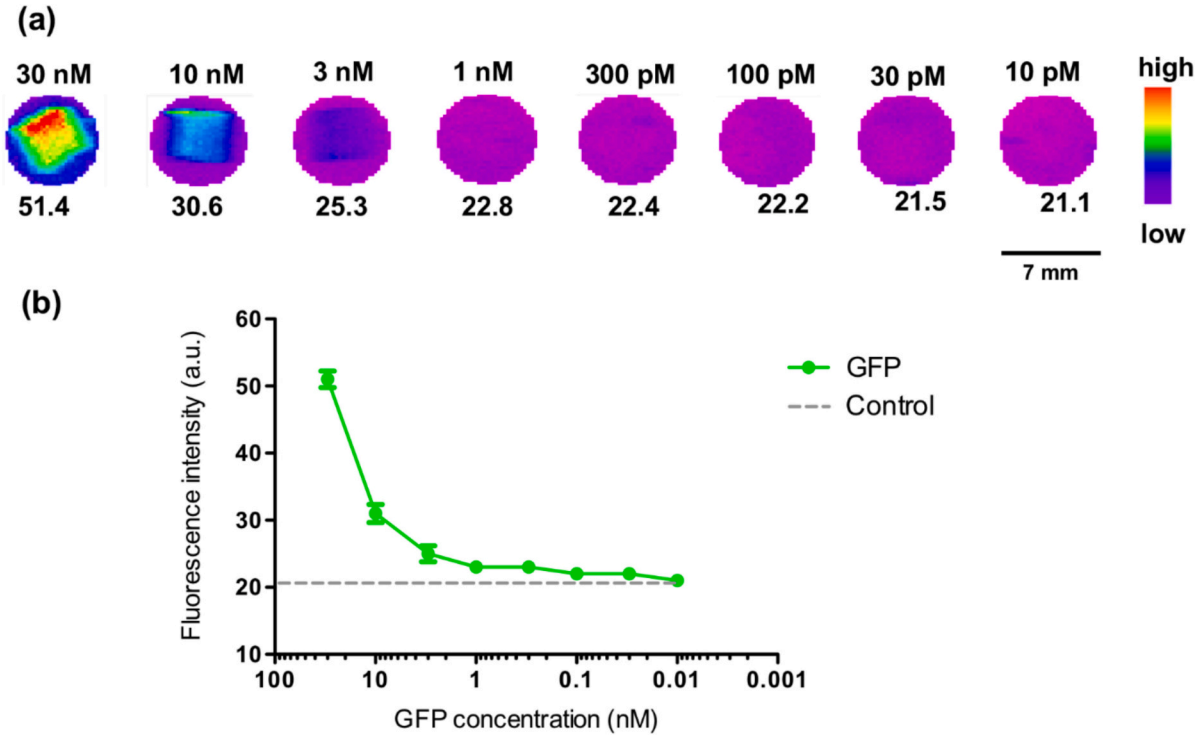

Fig. 8. Fluorescence measurements of nanostructured UNCD surfaces after TFAAD functionalization and immobilization of GFP from solutions with different concentrations: (a) average fluorescence of the whole well in arbitrary units for one series of measurements (out of 5). The average fluorescence of PBS solution used as control was 21 a.u. (b) average fluorescence determined from all measured samples (N = 5).

source and a reflectron type time-of-flight analyzer. UHV base pressure during analysis was $<2 \times 10^{-8}$ mbar. For high mass resolution the Bi source was operated in bunched mode providing Bi_3^+ primary ion pulses at 25 keV energy and 1.4 ns pulse length. The primary ion beam was rastered across a 500 × 500 μm^2 field of view on the sample, and 128 × 128 data points were recorded. Data acquisition was stopped at the quasi static limit (10^{11} ions/cm^2). Mass scale calibration was based on low Mw hydrocarbon signals or DLC derived signals.

3. Results and discussion

3.1. Nanostructured UNCD films with different surface terminations

UNCD films prepared under the same conditions were previously characterized by a variety of techniques and the results were presented elsewhere [43–49]. Briefly, they are composed of diamond nanocrystallites of up to 10 nm embedded in amorphous carbon matrix, as revealed by transmission electron microscopy (TEM) on samples deposited under the same conditions in earlier study [43]. The volume fraction of both phases (crystalline and amorphous) is close to unity. In addition to carbon, elastic recoil detection (ERD) analyses revealed for

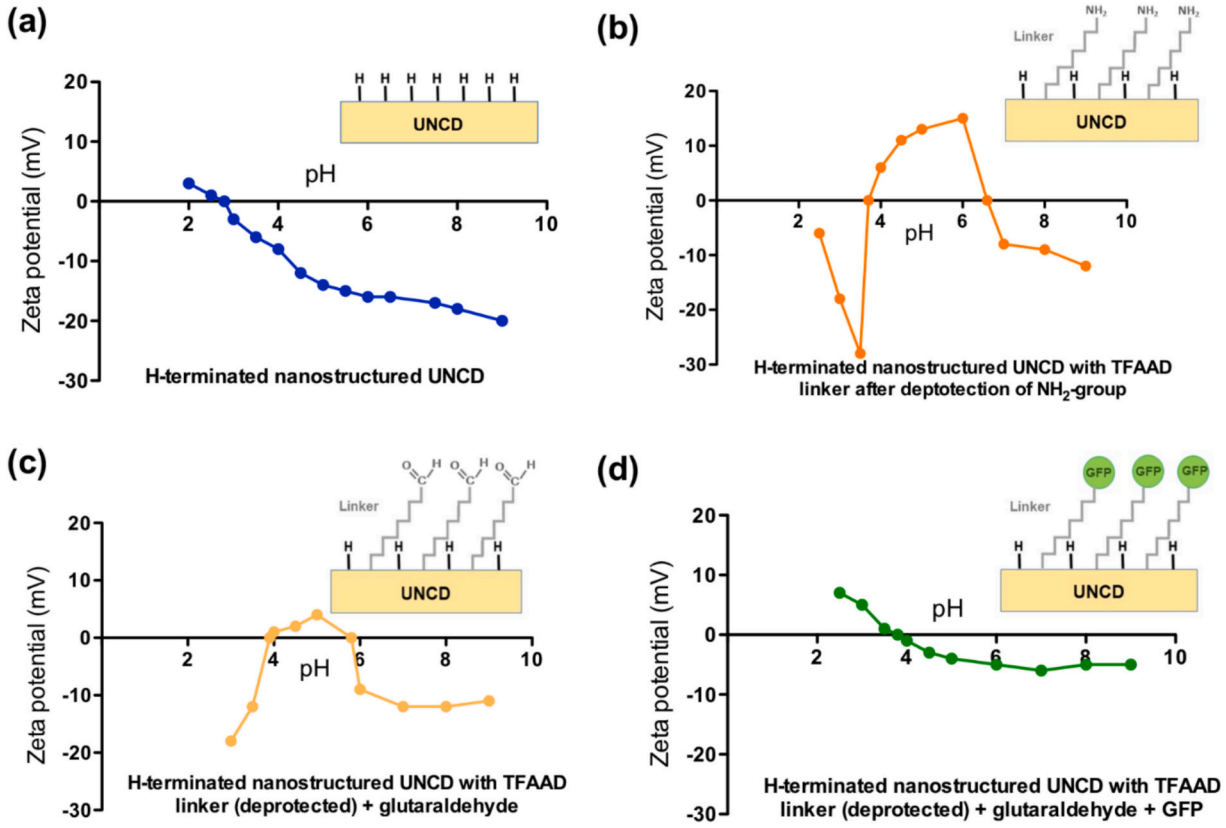

Fig. 9. Zeta potentials of (a) H-terminated nanostructured UNCD surface, (b) after functionalization with TFAAD linker and deprotection of the -NH_2 group, (c) after addition of glutaraldehyde and (d) after covalent immobilization of GFP.

such samples the presence in the bulk of nitrogen (1.1 at.%) and hydrogen (8.0 at.%) stemming from the source gas mixture and of oxygen (0.7 at.%) as contamination from the gas background [44]. The surface is hydrogen-terminated with H content of ca. 14 at.% as shown by former nuclear reaction analysis (NRA) [45]. In addition, X-ray photoelectron spectroscopy (XPS) detected the presence of oxygen and nitrogen on the surface of UNCD samples prepared under the same conditions in a previous investigation [47], which was supported by the measurements in the current study discussed below.

The surface roughness of the unstructured UNCD surface is on the order of 25 nm as determined by atomic force microscopy (AFM) (Fig. 3 (a)). The surface is rather smooth and the topography is dominated by rounded structures of ca. 150 nm as shown by AFM and scanning electron microscopy (SEM) (Fig. 3 (b)), which can be attributed to the growth mechanism of UNCD films with high secondary nucleation rate. The nanostructuring leads to formation of wrinkles (Figs. 3 (c) and (d)), which increase the rms roughness to 36 nm and respectively the area for interaction with proteins. Software Gwyddion was applied to estimate the enhancement of the surface area due to nanostructuring. The ratio of the real surface (31.14 μm^2 and 26.80 μm^2 for the nanostructured and unstructured surfaces, respectively) and the projected surface area (25 μm^2 for 5 × 5 μm^2) gives a factor of "area enhancement". It is 1.07 for the unstructured surface and 1.25 for the nanostructured one, indicating an enhancement in the surface area by 16.82 % after nanostructuring under the applied conditions. The plasma modifications applied for alternation of the surface termination did not affect the morphology of the unstructured and nanostructured UNCD films. The oxygen plasma treatment rendered the UNCD surface O-terminated with increased oxygen content from ca. 4 at.% to ca. 11 at.% [48], the trifluoromethane plasma F-terminated with fluorine content of ca. 22 at.% [49], as shown in earlier investigations. As observed in a previous work [34], the surface oxygen content increased to ca. 12 at.% after oxygen etch plasma for nanostructuring and was reduced to ca. 6 at.% after hydrogen plasma treatment. In the current study the surface oxygen content after hydrogen plasma treatment under the same conditions was 6.94 at.%, revealing that the H-termination was not completely restored.

The different surface terminations of the UNCD surfaces, both unstructured and nanostructured, had impact on the wettability assessed by contact angle (CA) measurements against deionized water. The results presented in Fig. 4 reveal the increase of CA from 7.4 ± 0.1° of O-terminated to 32.7 ± 0.1° and 74.8 ± 0.1° of H- and F-terminated unstructured UNCD surfaces, respectively. The oxygen plasma rendered the UNCD surface strongly hydrophilic, the F-containing plasma – hydrophobic. The nanostructuring had almost no effect on the measured contact angles, which were slightly lower for the hydrophilic surfaces or slightly higher for the hydrophobic ones: 5.7 ± 0.4°, 37.9 ± 0.2° and 79.9 ± 2.0° for the O-, H- and F-terminated nanostructured UNCD surfaces, respectively.

Fig. 5 presents the zeta potentials of unstructured and nanostructured UNCD surfaces with various terminations as a function of pH value. The zeta potential is the potential difference between the medium and the stationary layer of fluid attached to the surface. The results revealed isoelectric points (IEPs), i.e. the pH values at which the net charge is zero, of 3.8 and 2.8 for the unstructured and nanostructured H-terminated UNCD, respectively (Fig. 5 (a)). Above these pH values the zeta potential is negative for both surfaces. The surface charge formation on H-terminated samples is influenced by adsorption of ions from the medium primarily through van der Waals forces. At higher pH, the increased concentration of OH^- ions lead to a negative zeta potential due to their adsorption. Conversely, at very low pH, the high concentration of H^+ ions resulted in a positive zeta potential. The nanostructuring of the UNCD surface had a minor impact on the measured values within the pH range of 2.0 to 9.0.

Measurements of the zeta potential of O-terminated UNCD samples

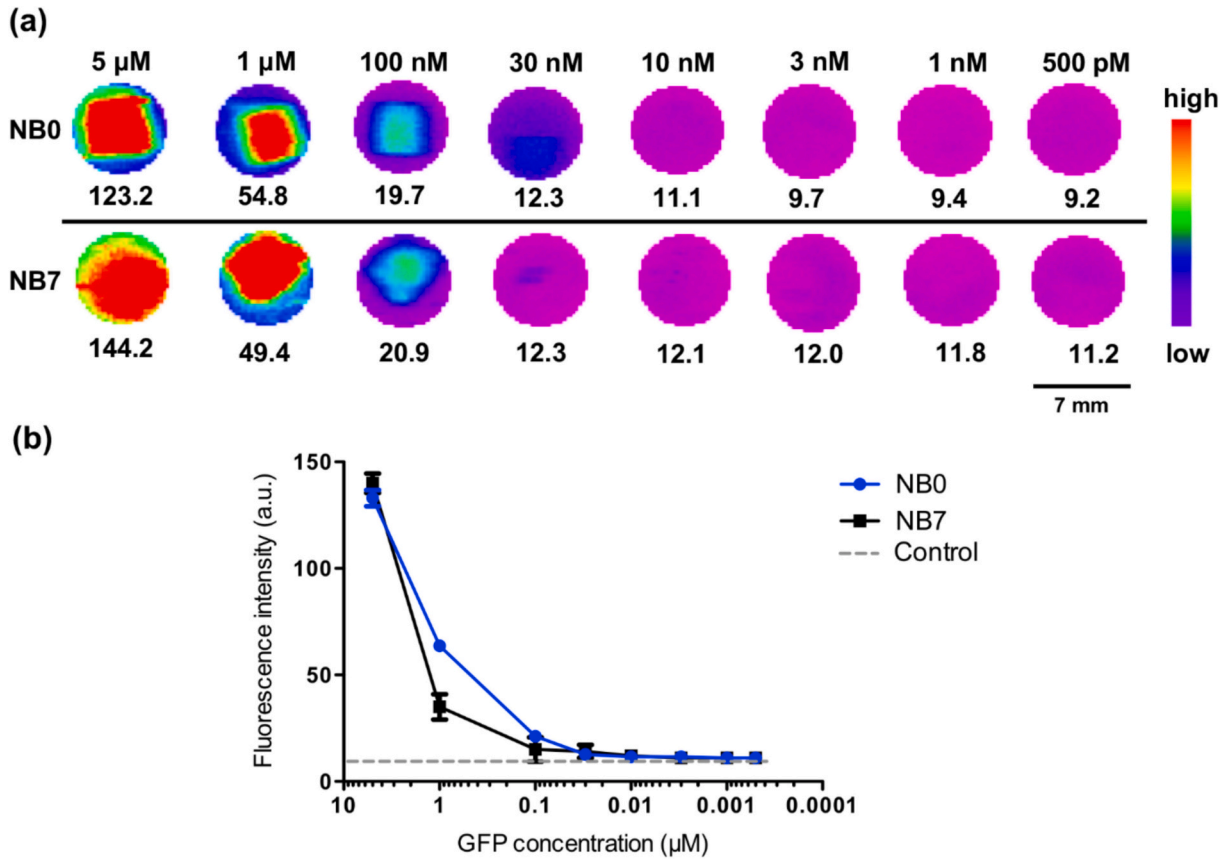

Fig. 10. Fluorescence measurements of UNCD samples with immobilized nanobodies NB0 and NB7 capturing GFP from solutions with different concentrations: (a) average fluorescence of the whole well in arbitrary units for one series of measurements (out of 5). The average fluorescence of PBS solution was 9.5 a.u. (b) average fluorescence determined from all measured samples (N = 5).

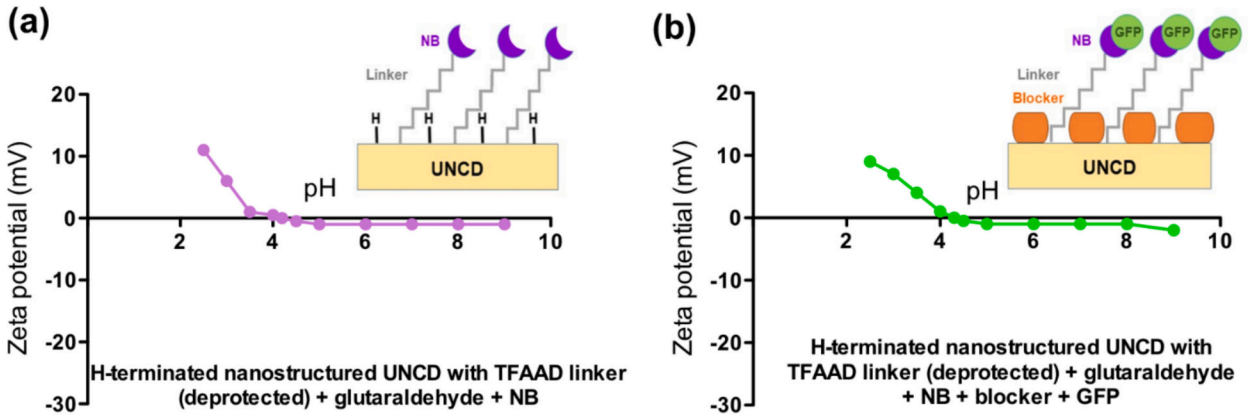

Fig. 11. Zeta potentials of UNCD samples (a) after immobilization of NB, and (b) after capturing of GFP from solution by the NB. In the second case blocker protein was also applied.

showed predominant positive values with IEP of 3.6 and 3.0 for the unstructured and nanostructured surfaces, respectively (Fig. 5 (b)). The zeta potential of a surface terminated with oxygen-containing groups (e.g., hydroxyl groups (OH), carbonyl groups (C=O), or ether groups (R-O-R)) is influenced by the acid-base reactions of these functional groups. Typically, at high pH values the surface acidic oxygen-containing groups become deprotonated, resulting in a negative charge, whereas at low pH the basic oxygen-containing groups are protonated, leading to a positive zeta potential. This expectation was confirmed by our previous zeta potential measurements of O-terminated UNCD surfaces which were performed between two identical samples forming a channel [33]. The measurements in the current study were performed utilizing only one sample with electric field applied to a single electrode which affect the measured zeta potential values. Since the surfaces with oxygen terminations showed low positive zeta potentials at high pH, this can be attributed to adsorption of Na^+ ions (from NaOH used to adjust pH), which contributed to a positive zeta potential. Conversely, the adsorption of Cl^- (from HCl used to adjust pH) resulted in a negative zeta potential at low pH. Both unstructured and nanostructured O-terminated UNCD surfaces exhibited lower variation of the zeta potential with pH changes.

The zeta potentials of F-terminated UNCD surfaces (Fig. 5 (c)) were

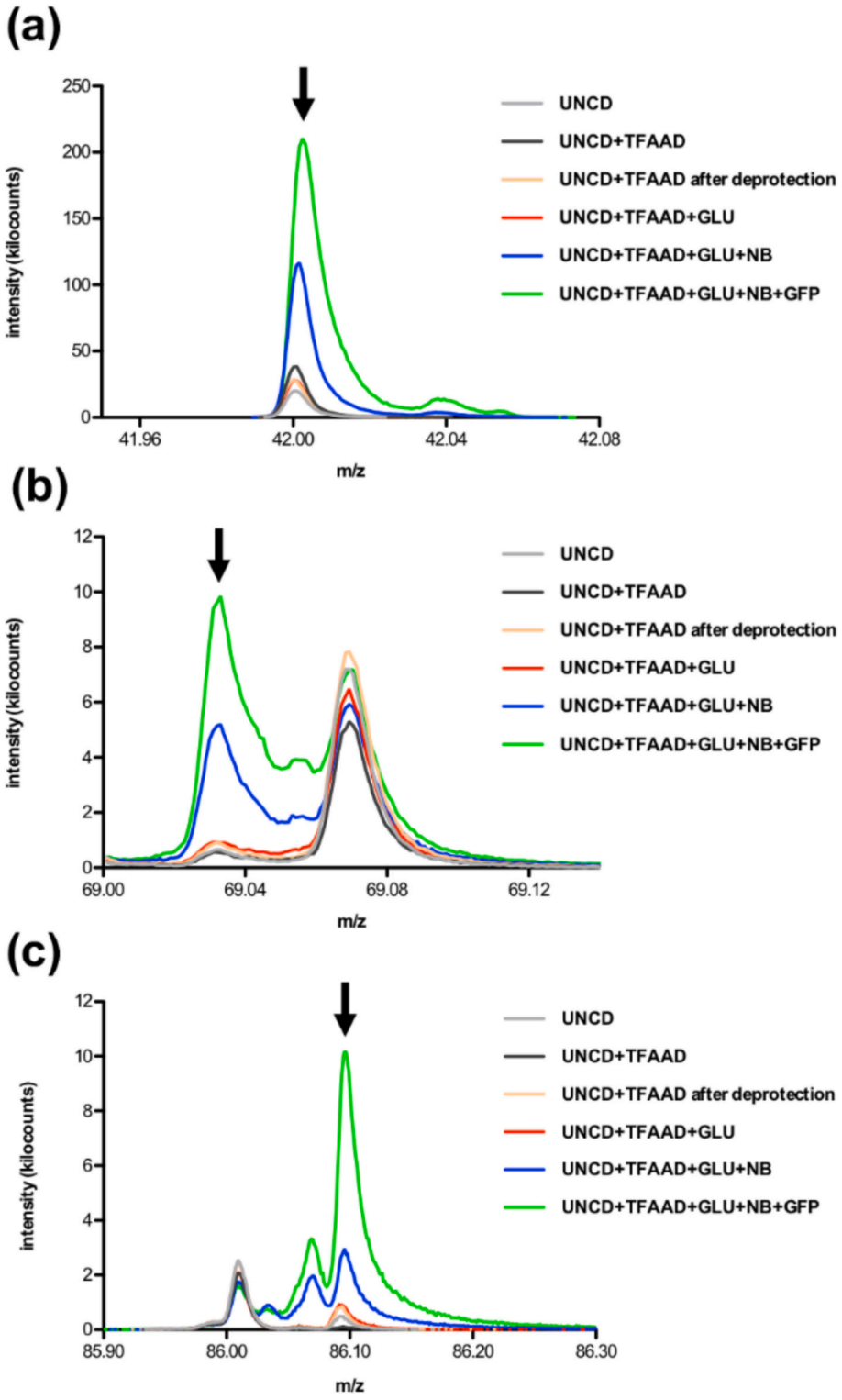

Fig. 12. ToF-SIMS peaks: (a) CNO^-, (b) $C_4H_5O^+$ from threonine and (c) $C_5H_{12}N^+$ from (iso)leucine detected after each step of the nanobody covalent immobilization and GFP capturing. The signal at *m/z* 69.07 in (b) is assigned to the alkyl fragment $C_5H_9^+$.

predominantly negative in the studied pH range with IEP of 2.2 for unstructured and 2.9 for nanostructured samples, most probably due to electron transfer from the aqueous solution to the UNCD surface [50–52]. The F-terminated samples showed a more significant change of the zeta potential across the pH range compared to H- and O-terminated samples.

Generally, the zeta potential varied significantly depending on the surface termination achieved via different plasma modifications, whereas the nanostructuring had a minor impact, which was observed also by the wettability. The O-terminated UNCD surface was positively charged, the H- and F-terminated ones negatively at the pH value of PBS solution (7.3) used as medium for the applied proteins.

Table 2
Concentration of O and N after individual steps of covalent immobilization of nanobodies and capturing of GFP as revealed by XPS.

Sample	Nanostr. UNCD	Nanostr. UNCD + TFAAD (protected)	Nanostr. UNCD + TFAAD (deprotected)	Nanostr. UNCD + TFAAD + GLU	Nanostr. UNCD + TFAAD + GLU + NB	Nanostr. UNCD + TFAAD + GLU + NB + GFP
N (at. %)	1.48	1.40	1.67	2.27	3.02	6.64
O (at. %)	6.94	7.76	8.07	9.39	14.49	13.91
F (at.%)	–	1.50	1.14	1.08	1.06	1.10

3.2. Non-covalent binding of GFP on unstructured and nanostructured UNCD surfaces with different terminations

The non-covalent binding of GFP with various concentrations on nanostructured UNCD surfaces with H-, O- and F-terminations was evaluated from the fluorescence intensity measured with a microplate reader. The results of the physical adsorption of GFP on various UNCD surfaces after 20 h incubation illustrated that in all cases the fluorescence intensity decreased with the GFP concentration (Fig. 6). In the lower concentration range (> 30 nM) the trend was less expressed which could be due to partial degradation of the protein during the long incubation time. The O-terminated UNCD samples incubated with GFP exhibited the highest intensity across the entire range of applied GFP concentrations from 10 μM to 500 pM, compared to the H- and F-terminated samples showing lower fluorescence. The oxygen plasma treatment rendered hydrophilic and slightly positively charged surfaces, as revealed by the contact angle and zeta potential measurements, shown above. In addition to the wettability of the UNCD surface, which plays an important role for the adsorption of proteins [53], the zeta potential also affects the process determining the degree of electrostatic repulsion or attraction of the proteins. The zeta potentials of the proteins used in the current work were also measured and the results are presented in Table 1. As seen, the zeta potentials of all proteins, including that of GFP, were negative at pH value of 7.0, which induced attraction to the positively charged O-terminated UNCD surface. On the other side, the H- and F-terminated UNCD surfaces, which possessed a negative zeta potential, did not enhance the physical adsorption of GFP on their surfaces, expressed by the lower fluorescence intensity measured on them. The results showed that the surface modifications of the UNCD samples affect differently the non-covalent GFP immobilization and can be selected to realize a surface which prone to such interaction or not.

As described above, H-terminated nanostructured UNCD surfaces were applied for functionalization with linker molecules and covalent immobilization of proteins. The fluorescence measurements showed that such surfaces cannot hinder the physical adsorption of GFP which was confirmed by ToF-SIMS and XPS. ToF-SIMS allows for specific detection of individual amino acids in proteins [59]. Since the used GFP is rich in isoleucine and leucine (5.0 and 8.4 %, respectively; the abundance of amino acids in the applied GFP and nanobodies is given in Supplementary Material S1), the characteristic $C_5H_{12}N^+$ secondary ion of these amino acids can be used to identify the non-covalent binding of GFP on nanostructured H-terminated UNCD surface, as seen in Fig. 7 (a). The XPS results for the chemical composition of these samples revealed an increased content of O (13.00 at.%) and N (10.24 at.%) after non-covalent immobilization of GFP compared to the nanostructured UNCD surface (6.94 at.% and 1.48 at.%, respectively). The normalized C1s spectrum of the sample in Fig. 7 (b) shows a shoulder peak at the higher binding energy side of the main peak (C-C/C-H bonds, 284.8 eV). The shoulder can be attributed to C-O/C-N bonds (ca. 286 eV) as well as to C=O bonds (around 288 eV) [60,61], all stemming from the amino acids of the GFP. The presence of physically adsorbed GFP on the H-terminated UNCD even after a thorough washing determine the necessity of blocker application, as discussed below, to occupy unspecific binding sites on the surface and assure covalent binding of the GFP via a linker.

3.3. Covalent binding of GFP on functionalized UNCD surfaces

UNCD samples with nanostructured surface and functionalized with TFAAD (see Fig. 2) were incubated for 20 h at 4 °C in GFP solutions with various concentrations: 30 nM, 10 nM, 3 nM, 1 nM, 300 pM, 100 pM, 30 pM, and 10 pM. After thorough washing to remove from the surfaces any non-covalently bonded proteins, the fluorescence of the samples was measured. As shown in Fig. 8, the fluorescence intensity decreased as the concentration of GFP was reduced, although this decrease did not follow a linear relationship, observed also in a previous study [34]. At higher concentrations (down to 3 nM), the average fluorescence intensity was significantly different for each sample. The immobilized protein remained fully functional and active (fluorescent), i.e. its structure remained intact [62]. At lower concentrations, especially with prolonged incubation times, GFP may become less stable or undergo degradation, resulting in fluorescence signal almost indistinguishable from that of the PBS solution used as a control.

To investigate the covalent immobilization of GFP at lower concentration (1 nM), samples were subjected to zeta potential measurements after each individual step, including the functionalization with TFAAD linker (see Fig. 2) and the results are presented in Fig. 9. The surface charge characteristics of nanostructured H-terminated UNCD exhibiting predominantly negative values (Fig. 9 (a)) was already discussed above. The attachment of TFAAD linker with deprotected -NH_2 group resulted in a change of the zeta potential which possessed two IEPs at pH of 3.7 and 6.6 with positive values between them (Fig. 9 (b)). This behavior of the zeta potential could be attributed to the effects of the adsorption of ions as well as to protonation of the -NH_2 functional group on the surface. The latter leading to the formation of -NH_3^+ seems to predominate at average pH values which resulted in positive zeta potential. At higher (above 6.6) pH values the ion adsorption (OH^-) governed the resulting surface charge, at lower (below 3.7) the functional groups might be (partly) damaged leading to negative surface charge. After the application of glutaraldehyde as a second linker, the zeta potential showed similar behavior to that observed for the samples with deprotected TFAAD (Fig. 9 (c)). One difference was the shift of IEPs for this sample to pH value of 3.9 and 5.8. In addition, the positive zeta potential between them lowered. It should be kept in mind that for this sample not only the aldehyde group from the glutaraldehyde, but also the -NH group from TFAAD contribute to the surface net charge together with the ion adsorption. The sample with covalently immobilized GFP exhibited a completely different behavior of the zeta potential with pH variation showing IEP at pH 3.8 and predominant low negative values approaching that of GFP as shown in Table 1 (Fig. 9 (d)). These results confirmed the successful immobilization of the protein on the UNCD surface.

3.4. Covalent immobilization of nanobodies on UNCD surfaces as GFP-binding proteins and application of blocker proteins

In a next series of experiments, the immobilization of nanobodies as capturing agents of GFP was investigated. To minimize the non-covalent binding of GFP on the UNCD surface, milk powder was applied as a blocker after the functionalization with the linker molecules. It is important that the blocking substance, after coupling, adsorbs to the still

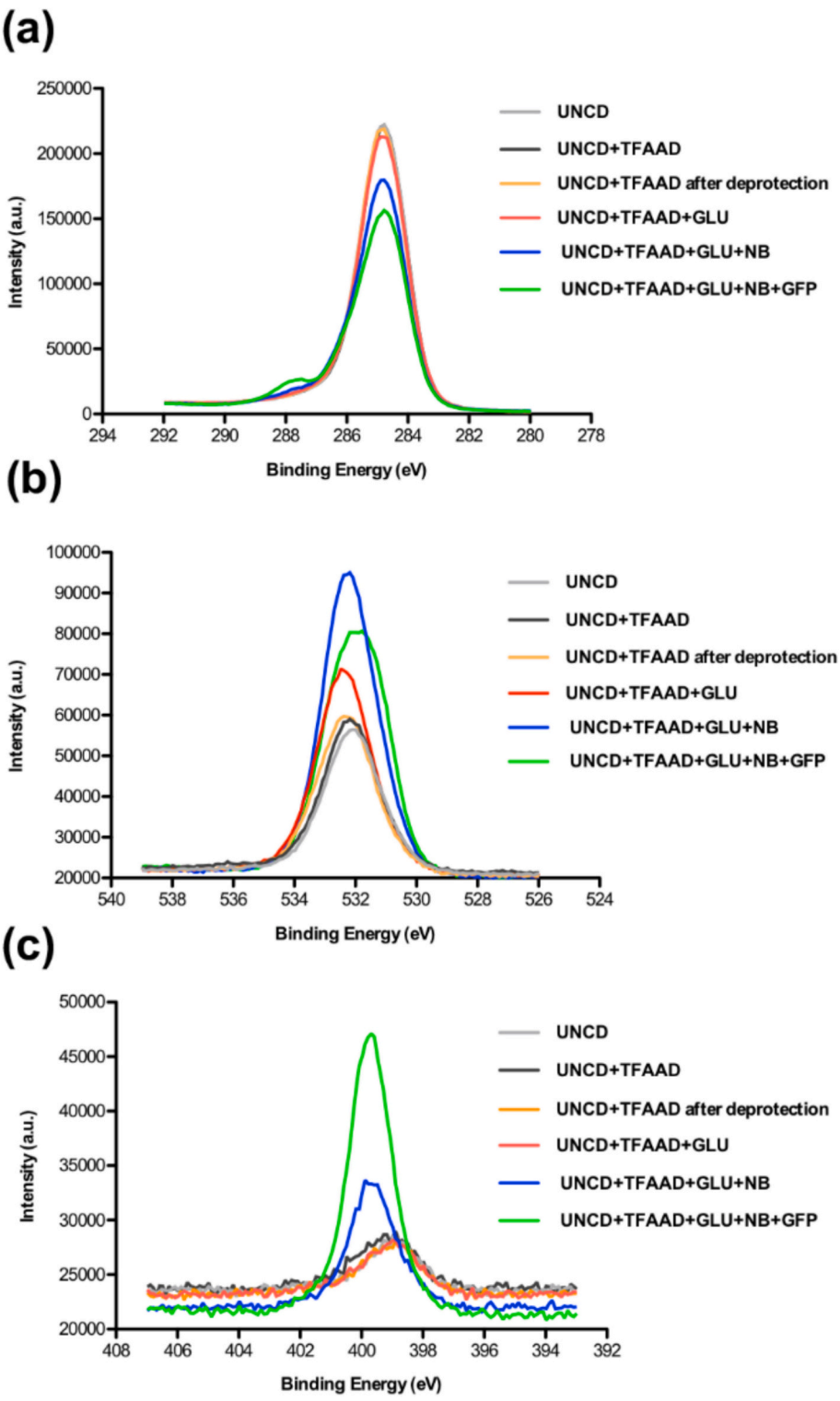

Fig. 13. XPS (a) C1s, (b) O1s and (c) N1s spectra of samples for individual steps of covalent immobilization of nanobody and capturing of GFP.

free sites of the surface, ideally forming a completely closed and dense layer. As next, two selected anti-GFP nanobodies (NB0 and NB7) were immobilized separately on UNCD surfaces and exposed to different concentrations of GFP. The fluorescence readings showed ca. 12-fold increase of the average intensity of the signal at the highest applied GFP concentration of 5 μM compared to the lower concentration range (Fig. 10). In this range (below 30 nM) the intensity of the signals was indistinguishable with the variation of the GFP concentration approaching that of the PBS solution used as a control, in a similar way as in the case of non-covalent immobilization of GFP discussed above. Furthermore, similar fluorescence intensities were found for both nanobodies NB0 and NB7 indicating that they captured equally well GFP from the solutions, despite having different epitopes and affinities towards it. The effect of the blocker for reduction of non-covalent GFP immobilization was also studied and the results are presented in Supplementary Material S2.

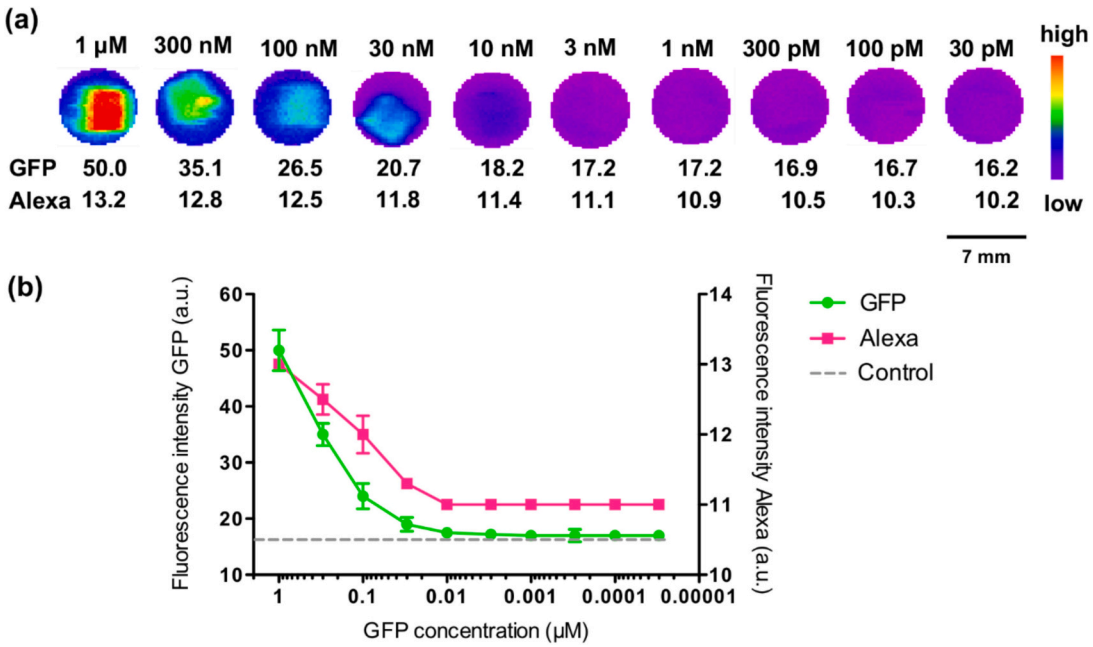

Fig. 14. Fluorescence measurements of UNCD samples with immobilized nanobody NB0 capturing GFP from solutions with different concentrations and additionally applied dye-labeled NB7: (a) average fluorescence (taken at the emission wavelength of GFP) of the whole well in arbitrary units for one series of measurements (out of 5). The average fluorescence of PBS solution was 16 a.u.; (b) average fluorescence (at the wavelengths of GFP and Alexa) determined from all measured samples (N = 5).

The zeta potentials of samples after the immobilization of NB and after capturing of GFP from solution (applying also a blocker) were measured and the results are presented in Fig. 11. Both samples exhibited similar trends to the GFP-immobilized sample (see Fig. 9 (d)). In general, the zeta potentials decreased initially with increasing pH, starting at ca. +10 mV at pH 2.5 reaching IEPs of 4.2 and 4.3 for the samples with NB before and after GFP capturing, respectively. With increasing pH value, the zeta potential of both samples remained almost constant. As shown in Table 1, the zeta potentials of all applied proteins were similar and after their immobilization they determined the surface charge reflecting the behavior of their ionizable groups at different pH levels. The proteins contain acidic (-COOH) and basic ($-NH_2$) groups, which can either lose or gain protons depending on the pH. At low pH, the carboxyl groups tend to be protonated (-COOH), and the amino groups typically gain protons ($-NH_3^+$), leading to a positive zeta potential. As the pH increases, these groups begin to deprotonate; the carboxyl groups become deprotonated ($-COO^-$) and the amino groups return to their neutral form ($-NH_2$), resulting in a more negative zeta potential. Around the IEP, the positive and negative charges are balanced.

Analogous samples, without application of blocker, were subjected to ToF-SIMS and XPS. Initially, the CNO^- secondary ion was registered after each step of the nanobody covalent immobilization and GFP capturing. As seen in Fig. 12 (a) its intensity increased firstly after the binding of the nanobody and secondly after that of GFP. For more detailed study, additional peaks were considered which can be used as markers for different amino acids with various abundance in each of the proteins (see Supplementary Material S1), namely $C_4H_5O^+$ for threonine and $C_5H_{12}N^+$ for (iso-)leucine. The intensity of both peaks increases after the binding of each of the proteins, however to a different extent (Fig. 12 (b) and (c)). The intensity increase of $C_4H_5O^+$ peak is lower since the nanobody contained slightly more threonine (8.1 %) than the GFP (6.3 %). On the other hand, the greater increase in the $C_5H_{12}N^+$ peak intensity can be attributed to significant contribution of the (iso-) leucine-rich GFP to the detected signal. The capturing of GFP can therefore be inferred not only from the total peak intensity but also from the intensity changes of specific peaks that can be aligned with the amino acid composition.

XPS measurements revealed increased content of O and N after each step of the immobilization of the nanobodies and the capturing of GFP (see Table 2). The C1s spectra of all samples are presented in Fig. 13 (a). They are dominated by a main peak at 284.8 eV attributed to C-C/C-H bonds. In the spectrum of the sample with immobilized nanobody a shoulder appears at the higher binding energy side of the main peak which can be assigned to the presence of C-O/C-N bonds (around 286 eV) as well as of C═O bonds (around 288 eV) stemming from the nanobody. After the capturing of GFP by the nanobody the intensity of the shoulder increases due to increased concentration of proteins on the sample. The O1s spectra in Fig. 13 (b) show peaks attributed to the presence of mainly C-O and C=O bonds, as indicated by the peak positions between 531.2 eV and 532.6 eV, whereas the N1s spectra (Fig. 13 (c)) reveal the increasing nitrogen content and a major peak at 399.85 eV related to the presence of amide groups in the samples with proteins. The fluorine content after functionalization with TFAAD was 1.50 at.% as determined by XPS and decreased to 1.14 at.% after deprotection, remaining almost unchanged during the next steps (see Table 2). The presence of F can be attributed to incomplete deprotection of all linker molecules and/or some contamination with the side product of the deprotection (OH-C-CF_3).

3.5. *Application of fluorescent reporter complex*

A reporter complex was created by labeling NB7 with Alexa Fluor dye 647. After purification the concentration of the labeled nanobodies was determined spectrophotometrically (90 μM) as well as the degree-of-labeling (DOL = 0.228) of the conjugate. The reporter complex was added to UNCD samples with immobilized NB0, applied blocker proteins and captured GFP from solutions with different concentrations, to which the complex should couple. The fluorescence signals of both GFP and Alexa were measured independently with the microplate reader due to their different excitation and emission wavelengths. As shown in Fig. 14 the fluorescence intensities followed similar trends with the variation of the GFP concentration: they decreased with decreasing the GFP concentration down to 1–3 nM and approached the detection limit at lower concentrations. The results demonstrate that a similar reporter complex

can be applied in case of non-fluorescent protein captured from solution by anti- or nanobody to monitor concentration variations.

4. Conclusions

This study investigates the immobilization and detection of green fluorescent protein (GFP) and GFP-specific nanobodies on UNCD surfaces, using both non-covalent and covalent strategies. The UNCD surfaces were either nanostructured by reactive ion etching or unstructured, with H-, O-, or F-terminations achieved via plasma treatments (H_2, O_2, CHF_3). The nanostructuring significantly increased the surface area for interaction, the plasma treatments altered the surface chemistry, affecting the wettability and the surface charge, without changing the surface morphology. Contact angle and zeta potential measurements showed that O-terminated surfaces were highly hydrophilic and positively charged, whereas H- and F-terminated surfaces were more hydrophobic and negatively charged. These differences strongly influenced the non-specific protein interaction.

Fluorescence measurements revealed that the nanostructured, O-terminated surfaces exhibited the highest non-specific GFP binding across all tested concentrations (between 10 μM and 500 pM), likely due to electrostatic attraction. The fluorescence signal intensity declined with decreasing the GFP concentration, approaching below 10 nM the background signal of the PBS control. For covalent immobilization of proteins, nanostructured UNCD surfaces were functionalized with TFAAD and glutaraldehyde. GFP immobilized via this route retained its fluorescence, indicating structural integrity and full function. Zeta potential measurements confirmed successful and stepwise surface functionalization and protein binding.

Highly specific anti-GFP nanobodies were immobilized for the first time on UNCD and used to capture GFP from solutions. Blocking any unsaturated binding sites with milk powder effectively suppressed non-specific interactions. Both tested nanobodies showed clear, concentration-dependent fluorescence signals, with up to a 12-fold increase of the signal intensity increasing the GFP concentration from 500 pM to 5 μM, demonstrating strong target specificity. Surface analyses (XPS, zeta potential, ToF-SIMS) at different stages confirmed successful immobilization of nanobodies and capture of GFP.

A key outcome of this work was the development of a fluorescence-based sandwich assay using a second anti-GFP nanobody labeled with a fluorophore. This reporter binds to already captured GFP, enabling dual fluorescence detection and quantification. For the first time, a nanobody was successfully applied in such a sandwich-format biosensor on a diamond surface. These results highlight the suitability of UNCD surfaces, as a robust, chemically stable platform for fluorescence-based biosensing, extending the application area of nanobodies [63,64]. The demonstrated sensitivity, specificity, and quantification capability position this system as a promising tool for detecting biologically relevant proteins, including non-fluorescent targets such as neuropeptides (e.g. pigment dispersing factor, PDF) involved in circadian rhythms of model organisms.

CRediT authorship contribution statement

Rezvaneh Ghasemitabesh: Writing – original draft, Investigation, Formal analysis, Data curation. **Daniel Merker:** Writing – original draft, Investigation, Data curation. **Jan W. Bröckel:** Writing – original draft, Investigation, Formal analysis, Data curation. **Daniela Bertinetti:** Writing – original draft, Methodology, Data curation. **Yahya Zakaria:** Methodology, Formal analysis, Data curation. **Alexander Welle:** Methodology, Formal analysis, Data curation. **Friedrich W. Herberg:** Writing – review & editing, Supervision, Resources, Funding acquisition. **Cyril Popov:** Writing – review & editing, Supervision, Project administration, Funding acquisition, Conceptualization.

Declaration of competing interest

The authors declare that they have no known competing financial interests or personal relationships that could have appeared to influence the work reported in this paper.

Acknowledgments

The authors would like to acknowledge the financial support by the German Research Foundation (DFG) funded Research Training Group "multiscale clocks" (448909517/GRK 2749 "Biological Clocks on Multiple Time Scales" to C. Popov and F.W. Herberg). They thank cordially Dr. Christoph Winkler from Anton Paar Germany GmbH for providing Litesizer DLS and SurPASS 3 instruments for all dynamic light scattering and zeta potential measurements presented in the current work as well as for the valuable instructions and fruitful discussion of the results. The authors acknowledge Vanessa Trouillet, Surface and Interface Analysis, KNMFi, IAM-ESS, Karlsruher Institut für Technologie (KIT), Germany for the XPS measurements, fruitful discussion for preparation of the samples and warm welcome to her lab. They extend their gratitude to Dr. Samir Mammadov, Thermo Fisher Scientific, for his continuous support of the work regarding the characterization of differently prepared bio-surfaces. Additionally, we thank Michaela Hansch, Oliver Bertinetti, Özge Efendi and Hai Hoang for assistance. The DNA of the nanobodies applied in the current work were provided by Prof. Jan Steyaert and his group, VIB-VUB Center for Structural Biology, Brussels, Belgium.

Appendix A. Supplementary data

Supplementary data to this article can be found online at https://doi.org/10.1016/j.diamond.2025.112432.

Data availability

Data will be made available on request.

References

[1] J.D. Newman, S.J. Setford, Enzymatic biosensors, Molecular Biotech. 32 (2006) 249–268, https://doi.org/10.1385/MB:32:3:249.
[2] I.V. da Silva Amatto, N.G. da Rosa-Garzon, F.A. de Oliveira Simões, F. Santiago, N. P. da Silva Leite, J.R. Martins, H. Cabral, Enzyme engineering and its industrial applications, Biotechnol. Appl. Biochem. 69 (2021) 289–409, https://doi.org/10.1002/bab.2117.
[3] D.D. Chaplin, Overview of the immune response, J. *Allergy Clin. Immunol.* 125 (2010) S345, https://doi.org/10.1016/j.jaci.2009.12.980.
[4] A.K. Mishra, R.A. Mariuzza, Insights into the structural basis of antibody affinity maturation from next-generation sequencing, Front. Immunol. 9 (2018) 117, https://doi.org/10.3389/fimmu.2018.00117.
[5] D.S. Hage, Immunoassays, Anal. Chem. 71 (1999) 294–304, https://doi.org/10.1021/a1999901+.
[6] E.P. Cipolatti, A. Valério, R.O. Henriques, D.E. Moritz, J.L. Ninow, D.M.G. Freire, E. A. Manoel, R. Fernandez-Lafuente, D. de Oliveira, Nanomaterials for biocatalyst immobilization – state of the art and future trends, RSC Adv. 6 (2016) 104675, https://doi.org/10.1039/c6ra22047a.
[7] D.V. Sotnikov, N.A. Byzova, A.V. Zherdev, B.B. Dzantiev, Retention of activity by antibodies immobilized on gold nanoparticles of different sizes: fluorometric method of determination and comparative evaluation, Nanomaterials 11 (2021) 3117, https://doi.org/10.3390/nano11113117.
[8] M. Meldal, S. Schoffelen, Recent advances in covalent, site-specific protein immobilization, F1000Research 5 (2016), https://doi.org/10.12688/f1000research.9002.1. Rev-2303.
[9] M. Shen, J.F. Rusling, C.K. Dixit, Site-selective orientated immobilization of antibodies and conjugates for immunodiagnostics development, Methods 116 (2017) 95–111, https://doi.org/10.1016/j.ymeth.2016.11.010.
[10] M. Sharafeldin, K. McCaffrey, J.F. Rusling, Influence of antibody immobilization strategy on carbon electrode immunoarrays, Analyst 144 (2019) 2108–2116, https://doi.org/10.1039/C9AN01093A.
[11] Y. Moskovitz, S. Srebnik, Conformational changes of globular proteins upon adsorption on a hydrophobic surface, Phys. Chem. Chem. Phys. 16 (2014) 11698–11707, https://doi.org/10.1039/c4cp00354c.
[12] F. Secundo, Conformational changes of enzymes upon immobilization, Chem. Soc. Rev. 42 (2013) 6250–6261, https://doi.org/10.1039/c3cs35495d.

[13] K. Chaudhary, K. Kumar, P. Venkatesu, D.T. Masram, Protein immobilization on graphene oxide or reduced graphene oxide surface and their applications: influence over activity, the structural and thermal stability of protein, Adv. Colloid Interf. Sci. 289 (2021) 102367, https://doi.org/10.1016/j.cis.2021.102367.
[14] K. Hernandez, R. Fernandez-Lafuente, Control of protein immobilization: coupling immobilization and site-directed mutagenesis to improve biocatalyst or biosensor performance, Enzym. Microb. Technol. 48 (2011) 107–122, https://doi.org/10.1016/j.enzmictec.2010.10.003.
[15] C. Mateo, J.M. Palomo, G. Fernandez-Lorente, J.M. Guisan, R. Fernandez-Lafuente, Improvement of enzyme activity, stability, and selectivity via immobilization techniques, Enzym. Microb. Technol. 40 (2007) 1451–1463, https://doi.org/10.1016/j.enzmictec.2007.01.018.
[16] R.C. Rodrigues, C. Ortiz, Á. Berenguer-Murcia, R. Torres, R. Fernández-Lafuente, Modifying enzyme activity and selectivity by immobilization, Chem. Soc. Rev. 42 (2013) 6290–6307, https://doi.org/10.1039/c2cs35231a.
[17] R.A. Hartvig, M. van de Weert, J. Østergaard, L. Jorgensen, H. Jensen, Protein adsorption at charged surfaces: the role of electrostatic interactions and interfacial charge regulation, Langmuir 27 (2011) 2634–2643, https://doi.org/10.1021/la104720n.
[18] K. Tamoliūnas, N. Galamba, Protein denaturation, zero entropy temperature, and the structure of water around hydrophobic and amphiphilic solutes, J. Phys. Chem. B 124 (2020) 10994–11006, https://doi.org/10.1021/acs.jpcb.0c08055.
[19] S. Smith, K. Goodge, M. Delaney, A. Struzyk, N. Tansey, M. Frey, A comprehensive review of the covalent immobilization of biomolecules onto electrospun nanofibers, Nanomaterials 10 (2020) 2142, https://doi.org/10.3390/nano10112142.
[20] M.Y. Mulla, L. Torsi, K. Manoli, Electronic biosensors based on EGOFETs, Methods Enzymol. 642 (2020) 403–433, https://doi.org/10.1016/bs.mie.2020.07.003.
[21] F. López-Gallego, J.M. Guisán, L. Betancor, Glutaraldehyde-mediated protein immobilization, Methods Mol. Biol. 1051 (2013) 33–41, https://doi.org/10.1007/978-1-62703-550-7_3.
[22] S.M. Mahdi Dadfar, S. Sekula-Neuner, V. Trouillet, M. Hirtz, Protein microarray immobilization via epoxide ring-opening by thiol, amine, and azide, Adv. Mater. Interfaces 8 (2021) 2002117, https://doi.org/10.1002/admi.202002117.
[23] C. Mateo, V. Grazu, J.M. Guisan, Immobilization of enzymes on monofunctional and heterofunctional epoxy-activated supports, Methods Mol. Biol. 1051 (2013) 43–57, https://doi.org/10.1007/978-1-62703-550-7_4.
[24] K. Yang, R.J. Narayan, Biocompatibility and functionalization of diamond for neural applications, Curr. Op. Biomed. Eng. 10 (2019) 60–68, https://doi.org/10.1016/j.cobme.2019.03.002.
[25] A.C. Taylor, C.H. González, B.S. Miller, R.J. Edgington, P. Ferretti, R.B. Jackman, Surface functionalisation of nanodiamonds for human neural stem cell adhesion and proliferation, Sci. Rep. 7 (2017) 7307, https://doi.org/10.1038/s41598-017-07361-y.
[26] Y. Dai, D.A. Proshlyakov, G.M. Swain, Effects of film morphology and surface chemistry on the direct electrochemistry of cytochrome *c* at boron-doped diamond electrodes, Electrochem. Acta 197 (2016) 129–138, https://doi.org/10.1016/j.electacta.2016.02.032.
[27] P.A. Nistor, P.W. May, Diamond thin films: giving biomedical applications a new shine, J. R. Soc. Interface 14 (2017) 20170382, https://doi.org/10.1098/rsif.2017.0382.
[28] D. Nidzworski, K. Siuzdak, P. Niedziałkowski, R. Bogdanowicz, M. Sobaszek, J. Ryl, P. Weiher, M. Sawczak, E. Wnuk, W.A. Goddard III, A. Jaramillo-Botero, T. Ossowski, A rapid-response ultrasensitive biosensor for influenza virus detection using antibody modified boron-doped diamond, Sci. Rep. 7 (2017) 15707, https://doi.org/10.1038/s41598-017-15806-7.
[29] S. Siddiqui, Z. Dai, C.J. Stavis, H. Zeng, N. Moldovan, R.J. Hamers, J.A. Carlisle, P. U. Arumugam, A quantitative study of detection mechanism of a label-free impedance biosensor using ultrananocrystalline diamond microelectrode array, Biosens. Bioelectron. 35 (2012) 284–290, https://doi.org/10.1016/j.bios.2012.03.001.
[30] X.L. Kong, L.C.L. Huang, C.M. Hsu, W.H. Chen, C.C. Han, H.C. Chang, High-affinity capture of proteins by diamond nanoparticles for mass spectrometric analysis, Anal. Chem. 77 (2005) 259–265, https://doi.org/10.1021/ac048971a.
[31] T.T.B. Nguyen, H.C. Chang, V.W.K. Wu, Adsorption and hydrolytic activity of lysozyme on diamond nanocrystallites, Diamond Rel. Mat. 4-7 (2007) 872–876, https://doi.org/10.1016/j.diamond.2007.01.030.
[32] E. Nicolau, J. Méndez, J. Fonseca, K. Griebenow, C.R. Cabrera, Bioelectrochemistry of non-covalent immobilized alcohol dehydrogenase on oxidized diamond nanoparticles, Bioelectrochem 85 (2012) 1–6, https://doi.org/10.1016/j.bioelechem.2011.11.002.
[33] D. Merker, M. Kesper, L.L. Kailing, F. Herberg, J.P. Reithmaier, I.V. Pavlidis, C. Popov, Nanostructured modified ultrananocrystalline diamond surfaces as immobilization support for lipases, Diam. Relat. Mater. 90 (2018) 32–39, https://doi.org/10.1016/j.diamond.2018.09.027.
[34] D. Merker, D. Bertinetti, R. Merz, M. Kopnarski, F.W. Herberg, C. Popov, Enhanced protein immobilization efficacy by nanostructuring of ultrananocrystalline diamond surface, Diam. Relat. Mater. 136 (2023) 109898, https://doi.org/10.1016/j.diamond.2023.109898.
[35] E.A. Della Pia, K.L. Martinez, Single domain antibodies as a powerful tool for high-quality surface plasmon resonance studies, PLoS One 10 (2015) e0124303, https://doi.org/10.1371/journal.pone.0124303.
[36] D. Schumacher, J. Helma, A.F.L. Schneider, H. Leonhardt, C.P.R. Hackenberger, Nanobodies: chemical functionalization strategies and intracellular applications, Angew. *Chem. Int. Ed.* 57 (2018) 2314–2333, https://doi.org/10.1002/anie.201708459.
[37] T. Tamura, Y. Kioi, T. Miki, S. Tsukiji, I. Hamachi, Fluorophore labeling of native FKBP12 by ligand-directed tosyl chemistry allows detection of its molecular interactions in vitro and in living cells, J. Am. Chem. Soc. 135 (2013) 6782–6785, https://doi.org/10.1021/ja401956b.
[38] B.N. Giepmans, S.R. Adams, M.H. Ellisman, R.Y. Tsien, The fluorescent toolbox for assessing protein location and function, Science 312 (2006) 217–224, https://doi.org/10.1126/science.1124618.
[39] A.D. Radadia, C.J. Stavis, R. Carr, H. Zeng, W.P. King, J.A. Carlisle, A. Aksimentiev, R.J. Hamers, R. Bashir, Control of the nanoscale environment to improve stability of immobilized proteins on diamond surfaces, Adv. Funct. Mater. 21 (2011) 1040–1050, https://doi.org/10.1002/adfm.201002251.
[40] N. Yang, H. Uetsuka, H. Watanabe, T. Nakamura, C.E. Nebel, Photochemical amine layer formation on H-terminated single-crystalline CVD diamond, Chem. Mater. 19 (2007) 2852–2859, https://doi.org/10.1021/cm070349m.
[41] B.P. Cormack, R.H. Valdivia, S. Falkow, FACS-optimized mutants of the green fluorescent protein (GFP), Gene 173 (1996) 33–38, https://doi.org/10.1016/0378-1119(95)00685-0.
[42] R. Huhnstock, M. Reginka, A. Tomita, M. Merkel, K. Dingel, D. Holzinger, B. Sick, M. Vogel, A. Ehresmann, Translatory and rotatory motion of exchange-bias capped Janus particles controlled by dynamic magnetic field landscapes, Sci. Rep. 11 (2021) 21794, https://doi.org/10.1038/s41598-021-01351-x.
[43] A. Voss, H. Wei, Y. Zhang, S. Turner, G. Ceccone, J.P. Reithmaier, M. Stengl, C. Popov, Strong attachment of circadian pacemaker neurons on modified ultrananocrystalline diamond surfaces, Mater. Sci. Eng. C 64 (2016) 278–285, https://doi.org/10.1016/j.msec.2016.03.092.
[44] W. Kulisch, C. Popov, Ultrananocrystalline diamond/amorphous carbon nanocomposite films for biotechnological applications, *Nanostructured Materials for Advanced Technological Applications*, NATO Science for Peace and Security Series - B: Physics and Biophysics, Springer, Dordrecht, Netherlands, 2009, ISBN 978-1-4020-9914-4, pp. 479–500.
[45] W. Kulisch, T. Sasaki, F. Rossi, C. Popov, C. Sippel, D. Grambole, Hydrogen incorporation in ultrananocrystalline diamond/amorphous carbon films, Phys. Status Solidi (RRL) Rapid Res. Lett. 2 (2008) 77–79, https://doi.org/10.1002/pssr.200701305.
[46] W. Kulisch, C. Popov, E. Lefterova, S. Bliznakov, J.P. Reithmaier, F. Rossi, Electrical properties of ultrananocrystalline diamond/amorphous carbon nanocomposite films, Diam. Relat. Mater. 19 (2010) 449–452, https://doi.org/10.1016/j.diamond.2010.01.021.
[47] J. Miksovsky, A. Voss, R. Kozarova, T. Kocourek, P. Pisarik, G. Ceccone, W. Kulisch, M. Jelinek, M.D. Apostolova, J.P. Reithmaier, C. Popov, Cell adhesion and growth on ultrananocrystalline diamond and diamond-like carbon films after different surface modifications, Appl. Surf. Sci. 297 (2014) 95–102, https://doi.org/10.1016/j.apsusc.2014.01.085.
[48] D. Merker, Y. Handzhiyski, R. Merz, M. Kopnarski, J.P. Reithmaier, C. Popov, M. D. Apostolova, Influence of surface termination of ultrananocrystalline diamond films coated on titanium on the response of human osteoblast cells: a proteome study, Mater. Sci. Eng. C 128 (2021) 112289, https://doi.org/10.1016/j.msec.2021.112289.
[49] W. Kulisch, A. Voss, D. Merker, J.P. Reithmaier, R. Merz, M. Kopnarski, C. Popov, Plasma surface fluorination of ultrananocrystalline diamond films, Surf. Coat. Technol. 302 (2016) 448–453, https://doi.org/10.1016/j.surfcoat.2016.06.029.
[50] J. Hees, A. Kriele, O.A. Williams, Electrostatic self-assembly of diamond nanoparticles, Chem. Phys. Lett. 509 (2011) 12–15, https://doi.org/10.1016/j.cplett.2011.04.083.
[51] L. Ginés, S. Mandal, A.-I. Ahmed, C.-L. Cheng, M. Sow, O.A. Williams, Positive zeta potential of nanodiamonds, Nanoscale 9 (2017) 12549–12555, https://doi.org/10.1039/C7NR03200E.
[52] V. Chakrapani, J.C. Angus, A.B. Anderson, S.D. Wolter, B.R. Stoner, G. U. Sumanasekera, Charge transfer equilibria between diamond and an aqueous oxygen electrochemical redox couple, Science 318 (2007) 1424–1430, https://doi.org/10.1126/science.114884.
[53] C. Popov, H. Vasilchina, W. Kulisch, F. Danneil, M. Stüber, S. Ulrich, A. Welle, J. P. Reithmaier, Wettability and protein adsorption on ultrananocrystalline diamond/amorphous carbon composite films, Diam. Relat. Mater. 18 (2009) 895–898, https://doi.org/10.1016/j.diamond.2009.02.004.
[54] M. Ormö, A.B. Cubitt, K. Kallio, L.A. Gross, R.Y. Tsien, S.J. Remington, Crystal structure of the Aequorea victoria green fluorescent protein, Science 273 (1996) 1392–1395, https://doi.org/10.1126/science.273.5280.1392.
[55] R.Y. Tsien, The green fluorescent protein, Annu. Rev. Biochem. 67 (1998) 509–544, https://doi.org/10.1146/annurev.biochem.67.1.509.
[56] RCSB Protein Data Bank, GFP Nanobody NMR Structure (PDB ID: 7V0V), Retrieved from, https://www.rcsb.org/structure/7v0v, 2021.
[57] S. Muyldermans, Nanobodies: natural single-domain antibodies, Annu. Rev. Biochem. 82 (2013) 775–797, https://doi.org/10.1146/annurev-biochem-063011-092449.
[58] C.G. (Kees) de Kruif, T. Huppertz, Casein micelles: size distribution in milks from individual cows, J. Agric. Food Chem. 60 (2012) 4649–4655, https://doi.org/10.1021/jf301397w.
[59] J.B. Lhoest, M.S. Wagner, C.D. Tidwell, D.G. Castner, Characterization of adsorbed protein films by time-of-flight secondary ion mass spectrometry, J. Biomed. Mater. Res. 57 (2001) 432–440, https://doi.org/10.1002/1097-4636.
[60] R. Al-Gaashani, A. Najjar, Y. Zakaria, S. Mansour, M.A. Atieh, XPS and structural studies of high quality graphene oxide and reduced graphene oxide prepared by different chemical oxidation methods, Ceram. Int. 45 (2019) 14439–14448, https://doi.org/10.1016/j.ceramint.2019.04.165.

[61] R. Al-Gaashani, Y. Zakaria, O.-S. Lee, J. Ponraj, V. Kochkodan, M.A. Atieh, Effects of preparation temperature on production of graphene oxide by novel chemical processing, Ceram. Int. 47 (2021) 10113–10122, https://doi.org/10.1016/j.ceramint.2020.12.159.

[62] A. Härtl, E. Schmich, J.A. Garrido, J. Hernando, S.C. Catharino, S. Walter, P. Feulner, A. Kromka, D. Steinmüller, M. Stutzmann, Protein-modified nanocrystalline diamond thin films for biosensor applications, Nat. Mater. 3 (2004) 736–742, https://doi.org/10.1038/nmat1204.

[63] T. Uchański, S. Masiulis, B. Fischer, V. Kalichuk, U. López-Sánchez, E. Zarkadas, M. Weckener, A. Sente, P. Ward, A. Wohlkönig, T. Zögg, H. Remaut, J.H. Naismith, H. Nury, W. Vranken, A.R. Aricescu, E. Pardon, J. Steyaert, Megabodies expand the nanobody toolkit for protein structure determination by single-particle cryo-EM, Nat. Methods 18 (2021) 60–68, https://doi.org/10.1038/s41592-020-01001-6.

[64] P. De Keyser, V. Kalichuk, T. Zögg, A. Wohlkönig, S. Schenck, J. Brunner, E. Pardon, J. Steyaert, A biosensor-based phage display selection method for automated, high-throughput Nanobody discovery, Biosens. Bioelectron. 271 (2025) 116951, https://doi.org/10.1016/j.bios.2024.116951.